*M*4 excitations of *p*-shell nuclei

N. G. Goncharova
Nuclear Physics Institute, Moscow State University, Moscow

Fiz. Elem. Chastits At. Yadra **23**, 1715–1769 (November–December 1992)

The studies of high-spin "stretched" states in light nuclei are reviewed. The results of the multiparticle shell model including particle–core coupling are compared with the experimental data for $M4$ transitions in p-shell nuclei. The decay properties, spectroscopic amplitudes, and energy distribution of the states arising as a result of $M4$ transitions are discussed.

INTRODUCTION

The experimental study of nuclei in reactions involving various test particles at intermediate energies has repeatedly extended the list of observed nuclear excitations. The objects of experimental and theoretical investigations now include new nuclear states with high spins, the discovery of which was impossible for small momentum transfers to the nucleus. The most interesting of these are nuclear excitations with the maximum value of the spin for a given $1\hbar\omega$ transition—the so-called "stretched" states.

The heuristic value of maximum-spin states (MSSs) became clear in the last 8–10 years when they were studied in reactions involving various test particles: (e,e'), (π,π'), (p,p') and (p,n) (see Ref. 1, for example). At the level of the doorway excitations, MSSs are formed owing to the transition of a nucleon with total angular momentum $j_1=l_1+1/2$ to a subshell with angular momentum $j_2=l_2+1/2$, where the total angular momentum of the excitation operator $J=J_{\max}=j_1+j_2=l_1+l_2+1$ is an even number. The parity of the excitation operator is negative and equal to $(-1)^L=(-1)^{J-1}$; stretched states arise owing to $MJ_{\max}$ transitions. In nuclei with $J_0=0$ only the set of states with spin $J_{\max}$ is excited. In nuclei with $J_0\neq 0$ the picture of $MJ_{\max}$ excitations is much more complicated: only states with $J=J_0+J_{\max}$ can be excited exclusively owing to $MJ_{\max}$ transitions. States of the excited nucleus with spins $J=J_0+J_{\max}-1,\ldots,|J_0-J_{\max}|$ are populated in inelastic scattering reactions not only by $MJ_{\max}$ excitations, but also owing to other multipole excitations, for example, $E(J_{\max}-1)$.

MSSs were first discovered in the reaction (e,e') on the ^{12}C nucleus (the 4^- state at energy 19.6 MeV) at Stanford.[2] The maximum spin of the excitation operator was fixed in the ^{208}Pb nucleus, where the $M14$ transition corresponds to the neutron particle–hole configuration $|i_{13/2}^{-1}j_{15/2}:14^-\rangle$.

It is interesting to study MSSs because they have several unique features:

1) Only the spin component of the nucleon nuclear current is responsible for excitation of $MJ_{\max}$ transitions. The contribution of the convection current to MSS excitation is zero. Upon MSS excitation, not only the nucleon spin but also the nucleon orbital angular momentum is flipped. The fact that the spin operator is responsible for MSS excitation in the approximation of a purely nucleon nuclear current makes these states a unique object for studying the spin and spin–isospin modes of nuclear excitations. In this respect MSSs can serve as a source of more accurate information than $M1$ resonances, since the convection nuclear current participates, albeit to a small degree, in the formation of magnetic dipole excitations. The problem of the behavior of the magnetic characteristics of nucleons in nuclear matter posed by investigators studying the magnetic moments and strengths of the magnetic resonances of lowest spin can be solved by studying states whose excitation is dominated by the nuclear magnetization current, i.e., Gamow–Teller resonances and stretched states of maximum spin.

2) The effective cross sections for MSS excitation in reactions involving various test particles are functions of a single spin transition density. Because of this, a comparative analysis of (e,e'), (π,π'), (p,p'), and (p,n) MSS excitation reactions makes it possible to separate nuclear structure effects from features of the dynamics of the interaction between the test particle and the nucleus. Comparison of such nucleon reactions with other ways of exciting MSSs leads to the possibility of determining the tensor component of the nucleon–nucleon interaction at large momentum transfers.

3) The simplicity of the structure of doorway MSS excitations and the possibility of extracting spectroscopic information from the analysis of reactions involving electrons and mesons make stretched states an object for which model approximations of nuclear theory can be tested.

The special possibilities for testing and improving theoretical models using MSSs are related to features of the structure of the doorway excitations corresponding to them. For self-conjugate nuclei the excitation of an MSS with a given isospin corresponds to a unique particle–hole configuration. Therefore, among the factors which jointly affect the structure and properties of multipole giant resonances (MGRs), in the case of stretched states one of the most important is missing: the mixing of doorway configurations. This makes it possible to obtain estimates of the role of other factors affecting the MGR properties which are more reliable than earlier ones. The problem of the relation between the nucleon and non-nucleon degrees of freedom of nuclei in the formation of MGRs and, in particular, in the suppression of the multipole excitation strengths is of great interest. The problem of MGR strength suppression was noticed even by investigators of

 0090-4759/92/060748-26$04.00

the giant dipole resonance and has been widely discussed in connection with the suppression of the strengths of magnetic resonances of lowest spin. Comparison of the experimental and theoretical values of the $MJ_{\max}$ transition strengths allows us to get a new look at the role of the nucleon degrees of freedom in forming the MGR strengths.

This review is devoted to the study of the high-spin states arising as a result of $M4$ transitions in p-shell nuclei.

In Sec. 1 we survey the possibilities offered by current experiments in electron and meson beams for determining the spectroscopic characteristics of the excited states arising as a result of $MJ_{\max}$ transitions.

Section 2 is devoted to the "particle–nuclear-final-state" (PNFS) version of the multiparticle shell model which allows a unified description of the MGR of nuclei with nonclosed shells. The results of theoretical calculations of $M4$ excitations of p-shell nuclei are compared with the features of the hole-state distribution over the levels of the final nuclei.

In Sec. 3 we study the partial characteristics of maximum-spin states of p-shell nuclei and compare the experimental and theoretical results for $M4$ excitations. The problem of suppression of the $M4$ transition strength in p-shell nuclei is discussed.

In the Conclusion we summarize the studies of $M4$ transitions and discuss possible improvements of the microscopic description of nuclear excitations.

1. EXCITATION OF $MJ_{\max}$ TRANSITIONS IN INELASTIC SCATTERING REACTIONS INVOLVING ELECTRONS AND HADRONS

The inelastic scattering of electrons on nuclei is a reliable method of studying excited nuclear states which is free from model assumptions about the interaction dynamics.

In the case of the scattering of an unpolarized electron beam on unpolarized nuclei the effective scattering cross section is related to the properties of the target nucleus through two form factors, the longitudinal (Coulomb) one F_L and the transverse one F_T (Refs. 3 and 4):

$$\frac{d^2\sigma}{d\Omega d\varepsilon}=\frac{Z^2\sigma_M}{\eta_R}\left\{\left(\frac{q_\mu^4}{q^4}\right)F_L^2(q,\varepsilon)+\left(\frac{1}{2}\frac{q_\mu^2}{q^2}+\tan^2\frac{\theta}{2}\right)F_T^2(q,\varepsilon)\right\}. \quad (1)$$

Here $\sigma_M=(\alpha^2\cos^2\theta/2)/(4\varepsilon_1^2\sin^4\theta/2)$ is the Mott scattering cross section, $\eta_R=1+(2\varepsilon_1\sin^2\theta/2)/M_T$ is the recoil factor, M_T is the target-nucleus mass, and θ is the scattering angle. The momentum transferred to the nucleus is $\vec{q}=(\vec{k}_1-\vec{k}_2)$, where $\vec{k}_1$ and $\vec{k}_2$ are the momenta of the incident and scattered electrons; $q_\mu^2=\vec{q}^2-\varepsilon^2$, where $\varepsilon=\varepsilon_1-\varepsilon_2$ is the excitation energy. Here and below we use the "natural" system $h=c=1$; $1\ \mathrm{F}^{-1}=197.33\ \mathrm{MeV}/c$. In the excitation of $MJ_{\max}$ transitions, $q\gg\varepsilon$ and $q_\mu^2\cong q^2$.

The charge density distribution in the nucleus affects the effective electron scattering cross section through the longitudinal form factor, and the dependence of the cross section on the distribution of the intranuclear current is concentrated in the transverse form factor. Since the form factors depend on q and ε but not on the scattering angle, the construction of the graph of the cross section as a function of θ for fixed q and ε (the Rosenbluth graph) allows the contributions of the longitudinal and transverse form factors to the cross section to be distinguished. Measurement of the cross sections at the scattering angle 180° isolates the transverse form factor:

$$\left.\frac{d^2\sigma}{d\Omega d\varepsilon}\right|_{\theta=180^\circ}=\frac{Z^2\alpha^2}{4\varepsilon_1^2}\left(1+\frac{2\varepsilon_1}{M_T}\right)^{-1}F_T^2(q,\varepsilon). \quad (2)$$

The transverse form factor is the sum of the multipole form factors of EJ and MJ transitions:

$$F_T^2(q,\varepsilon)=\sum_{J=1}\{F_{EJ}^2(q,\varepsilon)+F_{MJ}^2(q,\varepsilon)\}. \quad (3)$$

The multipole form factors F_{EJ} and F_{MJ} do not interfere, since the multipole operators generating them, $\hat{\mathscr{T}}^{\mathrm{el}}_{JM}$ and $\hat{\mathscr{T}}^{\mathrm{mag}}_{JM}$, have opposite parity: $(-1)^J$ for EJ and $(-1)^{J-1}$ for MJ. The multipole form factor corresponding to the EJ or MJ transition of the nucleus from the initial state $|J_i,T_i,M_{T_i},\alpha_i\rangle$ to the final state $|J_f,T_f,M_{T_f},\alpha_f\rangle$ is the matrix element of the corresponding operator of rank J, including the nuclear current-density operator $\hat{\vec{\mathscr{J}}}(\vec{r})$:

$$F_{EJ}=\frac{(4\pi)^{1/2}}{Z}(2J_i+1)^{-1/2}\times|\langle J_fT_fM_{T_f}\alpha_f\|\hat{\mathscr{T}}^{\mathrm{el}}_J\|J_iT_iM_{T_i}\alpha_i\rangle|; \quad (4)$$

$$\hat{\mathscr{T}}^{\mathrm{el}}_{JM}=\frac{1}{q}\int d^3r[\vec{\nabla}\times j_J(qr)\vec{Y}^M_{JJ1}(\Omega)]\hat{\vec{\mathscr{J}}}(\vec{r}); \quad (5)$$

$$F_{MJ}=\frac{(4\pi)^{1/2}}{Z}(2J_i+1)^{-1/2}\times|\langle J_fT_fM_{T_f}\alpha_f\|\hat{\mathscr{T}}^{\mathrm{mag}}_J\|J_iT_iM_{T_i}\alpha_i\rangle|; \quad (6)$$

$$\hat{\mathscr{T}}^{\mathrm{mag}}_{JM}=\int d^3r j_J(qr)(\vec{Y}^M_{JJ1}(\Omega)\hat{\vec{\mathscr{J}}}(\vec{r}). \quad (7)$$

In (5) and (7), $j_J(qr)$ are the spherical Bessel functions, $\vec{Y}^M_{JL}$ are the vector spherical harmonics ($\vec{L}=\vec{J}+\vec{l}$),

$$\vec{Y}^M_{JL}=\sum_{m=-L}^{L}\sum_{\mu=0,\pm1}(lm1\mu|JM)Y_{LM}\xi_\mu, \quad (8)$$

and ξ_μ are the axes of the cyclical basis.

The operators (5) and (7) are operators not only in configuration space, but also in isospin space. In the latter they represent the sum of an isoscalar and an isovector. Introducing the isospin reduction, for the multipole form factors we have

$$F_{KJ,T}=\frac{\sqrt{4\pi}}{Z}(2J_i+1)^{1/2}(2T_f+1)^{1/2}\times\langle T_iM_{T_i}TO|T_fM_{T_f}\rangle\times\langle J_fT_f\alpha_f||\,|B_{J,T}|\,||J_iT_i\alpha_i\rangle, \quad (9)$$

where $\hat{B}_J$ has the form (5) for EJ form factors and the form (7) for MJ form factors.

The nucleon nuclear current density is the sum of the convection and magnetization current densities:

$$\hat{\vec{\mathscr{J}}}(\vec{r})=\hat{\vec{\mathscr{J}}}^{\rm con}(\vec{r})+[\vec{\nabla}\times\vec{\mu}(\vec{r})]. \tag{10}$$

In addition to the nucleon components of the current density, the nuclear current must also contain contributions from non-nucleon degrees of freedom of the nucleus; in the range of momentum and energy transfers considered the non-nucleon degrees of freedom are manifested as meson exchange currents (MECs).[5]

In microscopic models of the nucleus the matrix elements of multipole operators are calculated in the point-nucleon approximation, where the multipole operators are linear combinations of the single-particle operators:

$$\hat{\mathscr{T}}^{\rm el}_{JM}=\frac{q}{2M}\sum_i\left\{\hat{\mu}_i j_J(qr_i)[Y_J\times\vec{\sigma}_i]_{JM}\right.$$
$$+\frac{2\hat{e}_i}{q}\left[\sqrt{\frac{J+1}{2J+1}}\,j_{J-1}(qr_i)[Y_{J-1}\times\vec{\nabla}_i]_{JM}\right.$$
$$\left.\left.-\sqrt{\frac{J}{2J+1}}\,j_{J+1}(qr_i)[Y_{J+1}\times\vec{\nabla}_i]_{JM}\right]\right\}. \tag{11}$$

$$\hat{\mathscr{T}}^{\rm mag}_{JM}=\frac{iq}{2M}\sum_i\left\{\hat{\mu}_i\left[\sqrt{\frac{J+1}{2J+1}}\,j_{J-1}(qr_i)[Y_{J-1}\times\vec{\sigma}_i]_{JM}\right.\right.$$
$$\left.-\sqrt{\frac{J}{2J+1}}\,j_{J+1}(qr_i)[Y_{J+1}\times\vec{\sigma}_i]_{JM}\right]$$
$$\left.-\frac{2e_i}{q}\,j_J(qr_i)[Y_J\times\vec{\nabla}_i]_{JM}\right\}. \tag{12}$$

In (11) and (12), $\hat{e}_i$ and $\hat{\mu}_i$ are operators in isospin space,

$$\hat{e}_i=e_0+e_1\hat{\tau}_{3i}=\frac{1+\hat{\tau}_{3i}}{2};$$
$$\hat{\mu}_i=\mu_0+\mu_1\hat{\tau}_{3i}=\frac{\mu_p+\mu_n}{2}+\frac{\mu_p-\mu_n}{2}\tau_{3i}, \tag{13}$$

μ_p and μ_n are the proton and neutron magnetic moments in nuclear magnetons, and M is the nucleon mass.

The finite size of the nucleon is usually taken into account in the calculations by introducing into the right-hand sides of Eqs. (4), (6), and (9) the form factors f_{SN}, which approximately reflect the growth of the effect of the nucleon size on the nuclear response function as the momentum transferred to the nucleus increases. The form factor for the finite-size nucleon is often written as[6]

$$f_{SN}=(1+q^2/q_N^2)^{-1},\quad q_N=855\ \text{MeV}. \tag{14}$$

If as the wave functions of the initial and final nuclear states we use the shell-model functions depending on $3A$ spatial coordinates, a correction f_{CM} is introduced into the expression for the form factors to take into account the nuclear center-of-mass motion. If as the nucleon wave functions we take the wave functions of the three-dimensional harmonic-oscillator potential (the HOWFs), then

$$f_{CM}=\exp\left[\frac{1}{A}\left(\frac{qb}{2}\right)^2\right], \tag{15}$$

where b is the oscillator parameter.

The formalism for calculating multipole form factors described briefly in this section is based on the Born approximation using plane waves. The higher the charge of the target nucleus, the larger the distortions of the electron waves in the field of the nucleus; the cross sections must be calculated in an approximation taking into account the distortion effect. Distortions are small for light nuclei, so the results can be compared with the plane-wave calculation by shifting the experimental points upwards on the momentum-transfer axis, since the Coulomb attraction accelerates the incident electron and focuses the electron wave:

$$q\to q_{\rm eff}=q\left(1+\frac{3\alpha Z}{2\varepsilon_1 R}\right), \tag{16}$$

where R is the radius of the target nucleus. As a rule, the experimental data obtained in (e,e') scattering are quoted for the values of $q_{\rm eff}$.

The multipole operators $\hat{\mathscr{T}}^{\rm el}_{JM}$ and $\hat{\mathscr{T}}^{\rm mag}_{JM}$ responsible for electroexcitation of EJ and MJ transitions are linear combinations of products of operators depending on the spatial and spin–angular variables and the isospin:

$$\hat{B}_{JM_J}=\sum_{i,T}\hat{O}_{JM_J,TM_T}(i)\hat{\tau}^T_{M_T}(i), \tag{17}$$

where $\hat{O}$ is a tensor operator of rank J with possible parametric dependence on T and M_T; $\tau^0=1$ and $\tau^1=\vec{\tau}$ are operators in isospin space. It is convenient to separate the matrix elements of single-particle tensor operators from the spectroscopic features of states of particular nuclei; the characteristic response of a particular nucleus to a single-particle multipole excitation is the multipole spectroscopic amplitude. In the literature there are several definitions of the spectroscopic amplitudes:[7]

$$\mathscr{Z}_{J,TM_T}(j_fj_i)$$
$$=(2J+1)^{1/2}(2J_i+1)^{-1/2}\langle J_fT_fM_{T_f}\alpha_f$$
$$\times\|[a_f^+\times a_i]_{J,TM_T}\|J_iT_iM_{T_i}\alpha_i\rangle, \tag{18}$$

or

$$S_{J,TM_T}=\langle J_fT_fM_{T_f}\alpha_f\|[a_f^+\times a_i]_{J,TM_T}\|J_iT_iM_{T_i}\alpha_i\rangle. \tag{19}$$

Here a^+ and a are creation and absorption operators, with

$$[a_f^+\times a_i]_{JM_J,TM_T}$$
$$\equiv[a^+_{j_fm_ft_{zf}}\times a_{j_im_it_{zi}}]_{JM_J,TM_T}$$
$$=\sum_{t_{zf}t_{zi}}\sum_{m_fm_i}(-1)^{1/2-t_{zi}}\langle\tfrac{1}{2}t_{zf}\tfrac{1}{2}-t_{zi}|TM_T\rangle$$
$$\times(-1)^{j_i-m_i}\langle j_fm_fj_i-m_i|JM_J\rangle a^+_{j_fm_ft_{zf}}a_{j_im_it_{zi}}. \tag{20}$$

In what follows we will mostly discuss nuclear-charge conserving (e,e') and (π,π') reactions. Therefore, the index

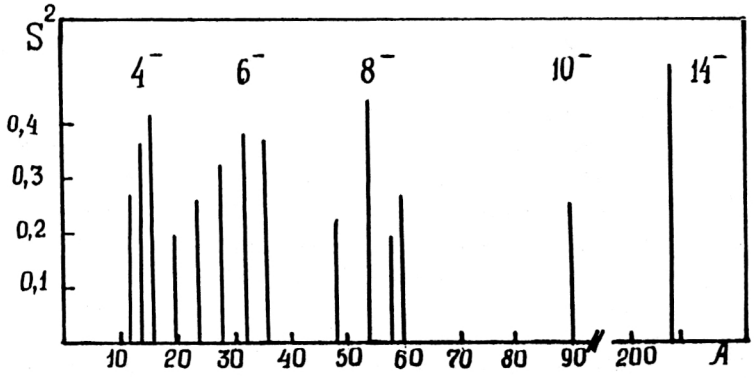

FIG. 1. Distribution of $S^2=F_T^2/(F_T^2)_{\text{lim}}$ (Refs. 1 and 9).

$M_T=0$ will be omitted. The relation between the spectroscopic amplitudes with $M_T=0$ and the amplitudes with $M_T=\pm 1$ is determined by the ratio of the corresponding vector-addition coefficients:

$$\mathscr{Z}_{M_T=\pm 1}=\frac{\langle T_i M_{T_i} 1 \pm 1 | T_f M_{T_f}\rangle}{\langle T_i M_{T_i} 10 | T_f M_{T_f}\rangle}\mathscr{Z}_{M_T=0}. \tag{21}$$

The definition (18) leads to the sum rule

$$\sum_{J_f,\alpha_f}\mathscr{Z}^2_{J,T=0}=1, \tag{22}$$

$$\sum_{J_f,\alpha_f,T_f=|\vec{T}_i+\vec{1}|}\mathscr{Z}^2_{J,T=1}=1. \tag{23}$$

The reduced matrix element of the operator (17) in the space of the nuclear wave functions can be expressed in terms of the spectroscopic amplitudes and matrix elements of single-particle operators in the space of the nucleon wave functions:[1)]

$$\langle J_f M_{T_f} T_f \alpha_f \| \hat{B}_{J,T} \| J_i T_i M_{T_i} \alpha_i\rangle$$

$$=\sum_{i,i_f,j_i}\langle j_f \| \hat{O}_J(i) \| j_i\rangle \sqrt{2}(2J_1+1)^{1/2}\mathscr{Z}_{J,T}(j_f j_i). \tag{24}$$

The operator O_{JM_J} contains both radial and spin–angular variables. The spin and angular dependences of the matrix elements of the operators is the same for a number of nuclear reactions, while the radial dependence is related to the dynamics of a particular reaction.[8] There are two types of operator corresponding to multipole excitations of nuclei in electromagnetic interactions:

$$\begin{aligned} O_{JM_J}&=f_J(r)Y_{JM_J}(\Omega),\\ O_{JM_J}&=f_J(r)[Y_L\times\vec{\nabla}]_{JM_J},\\ O_{JM_J}&=f_J(r)[Y_L\times\vec{\sigma}]_{JM_J}. \end{aligned} \tag{25}$$

The $MJ_{\max}$ excitations correspond only to operators of the third type. For $L=J-1$, Eq. (12) contains only a single term:

$$\hat{\mathscr{T}}^{\text{mag}}_J=\frac{iq}{2M}(\mu_0+\mu_1\hat{\tau}_3)\left\{\sqrt{\frac{J+1}{2J+1}}j_{J-1}(qr)[Y_{J-1}\times\vec{\sigma}]_J\right\}. \tag{26}$$

The transverse form factor of inelastic scattering of electrons at 180° corresponding to excitation of $MJ_{\max}$ transitions is a function of the spin transition density:

$$\rho^s_J(q)=\langle j_f \| j_{J-1}(qr)[Y_{J-1}\times\vec{\sigma}]_J \| j_i\rangle. \tag{27}$$

The dependence of the form factor on the spectroscopic amplitudes and the spin transition density is particularly simple for nuclei with $J_0=0$:

$$F_T^2(q)=\frac{4\pi}{Z^2}f^2_{SN}f^2_{CM}(J+1)$$

$$\times\left|\frac{q}{2M}\sum_{T=0,1}\sqrt{2}\mu_T\mathscr{Z}_{JT}\rho^s_J(q)\right|^2. \tag{28}$$

The systematic study of MGRs is based on the use of nucleon wave functions in the three-dimensional harmonic-oscillator potential (HOWFs). The use of HOWFs in the calculation (28) leads to the following dependence of the form factor on the momentum transferred to the nucleus:

$$F_T^2(q)\sim q^{2J}\exp(-b^2q^2/2). \tag{29}$$

Since $\mu_0/\mu_1=0.187$, isovector transitions dominate in inelastic electron scattering. Comparison of the theoretical calculations carried out using the particle–hole model of $MJ_{\max}$ excitations with the experimental data has shown that Eq. (29) reproduces the behavior of the experimental form factor up to momentum transfers of about 2.5 F^{-1}. However, the theoretical estimates greatly overestimate the value of the form factors: the ratio $S^2=F^2_{\text{exp}}/F^2_{\text{lim}}$, where F_{lim} is the $MJ_{\max}$ form factor calculated in the "limiting" particle–hole model, is considerably smaller than unity (Fig. 1). In Fig. 1 we show only several estimates of S^2 which illustrate the features of the distribution of this ratio. The factor S^2 depends not only on the filling of the subshell from which the nucleon transition starts, but also on the filling of the higher subshell with the same orbital angular momentum, the nucleons of which do not participate in the formation of doorway $MJ_{\max}$ excitations. The dependence of S^2 (and, accordingly, of the form factor of the $MJ_{\max}$ transition) on the subshell filling follows from the tendency for S^2 to grow within the p shell for the 4^- states of the ^{12}C, ^{14}C nuclei (the 4^-, $T=2$ state at 24.4 MeV) and the ^{16}O nucleus (the 4^-, $T=1$ state at 18.98 MeV) shown

in Fig. 1. A similar growth of S^2 is observed in the filling of the $1d_{5/2}$ subshell in the formation of the 6^-, $T=1$ state (the nuclei ^{20}Ne, ^{24}Mg, and ^{28}Si). Further increase of the number of nucleons in the $1d$–$2s$ shell leads to significant fragmentation of the $M6$-transition strength: for the ^{32}S nucleus in the (e,e') experiment of Ref. 10, nine states were found whose form factors have the momentum-transfer dependence characteristic of $M6$. Even for the most intense of these states the value of F_T^2 is roughly half that of F_T^2 for the 6^-, $T=1$, $E=14.36$ MeV state of the ^{28}Si nucleus, but the sum of all the form factors of the 6^-, $T=1$ states of the ^{32}S nucleus is 0.71 of F_{lim}^2, whereas for ^{28}Si this ratio is only 0.31. It should be noted that in the measurements of the multipole-strength distribution of ^{28}Si in Ref. 11 the 6^- levels with low intensity could be omitted, whereas in the recent experiment at NIKHEF (Ref. 10) even weak peaks of the (e,e') cross section were identified with high resolution. The role of spectator nucleons in nuclei of the $1d$–$2s$ shell is manifested even more clearly in the fact that measurement of the (e,e') cross sections for the ^{40}Ca nucleus has not yet revealed any noticeable intensity of 6^-, $T=1$ states. The 6^- level in ^{40}Ca was discovered in the (p,n) charge-exchange reaction,[12,13] but its intensity is very low. Significant fragmentation of $M8$ transitions has been seen for nuclei with a valence $1f$ shell.[14–18] The observed MSS fragmentation is not as large for heavy nuclei as for intermediate ones, and at the same time the estimates of S^2 for them are higher.

The relation between the experimental value of the $MJ_{\max}$-transition strength and its theoretical estimate (the so-called strength suppression) reflected in Fig. 1 is also typical for MGRs of other multipole orders. In connection with the strength suppression of Gamow–Teller resonances, there has been a great deal of discussion about the idea of redistribution of the transition strength along the energy axis owing to the contribution of non-nucleon degrees of freedom of the nucleus. In the case of Gamow–Teller resonances the dominant role is played by Δ-isobar excitation in nuclei, as suggested in Ref. 19. The role of non-nucleon degrees of freedom for $MJ_{\max}$ transitions has been studied by a number of authors (Refs. 20–22). They include the contributions of three types of graph:

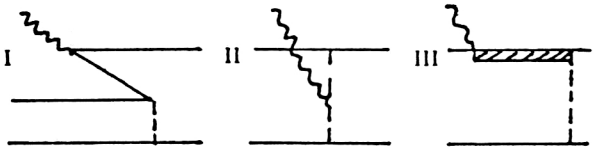

(30)

The results of these estimates are summarized in Fig. 2, where the ratio $(F_\sigma+F_{\text{I}}+F_{\text{II}})^2/F_\sigma^2$ and $(F_\sigma+F_{\text{I}}+F_{\text{II}}+F_{\text{III}})^2/F_\sigma^2$ is shown for the momentum transfer 1.8 F^{-1} (Refs. 20–22). The contribution of graph III, i.e., Δ-isobar excitation, was included in Ref. 22. In Fig. 3 we show the contributions of various graphs to the form factor for the 4^-, $T=1$ state of the ^{14}C nucleus according to the data of Ref. 23. The form factors shown by the dashed line have sign opposite to that of the spin form

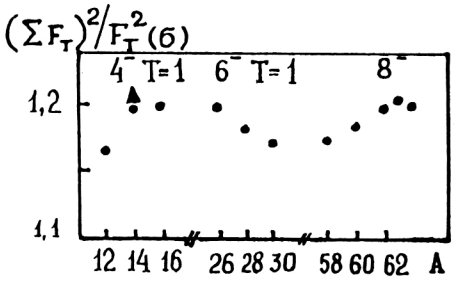

FIG. 2. MEC enhancement of transverse MSS form factors (Refs. 20 and 21).

factor (28), and the solid lines show $F_T(\sigma)$ and the form factors having the same sign. In the end, the inclusion of MECs for $MJ_{\max}$ transitions does not eliminate the suppression problem, but makes it worse: the theoretical value of the form factor increases by 15–20% when MECs are included.

An important aspect of studying MSSs is related to the fact that a single spin-multipole operator $[Y_{J-1}\times\vec{\sigma}]_J$ is responsible for exciting them in reactions involving electrons and hadrons. Of course, this universality of the excitation operator is approximate; it depends on the validity of the hypothesis of the one-step hadron–nucleus interaction mechanism. When this approximation is applicable, the differential cross section for excitation of $MJ_{\max}$ transitions in pion inelastic scattering on nuclei can be expressed in terms of the same transition density ρ_J^s as the cross section for the (e,e') reaction:

$$\left.\frac{d\sigma}{d\Omega}\right|_{(\pi,\pi')} = \frac{m_\pi^2}{\pi}\alpha_\pi^2(k_\pi/q)^4(J+1)\sin^2\theta \times\left|\sum_{T=0,1} t_T^{LS}(q)\mathscr{Z}_\pi\rho_J^s\right|^2. \tag{31}$$

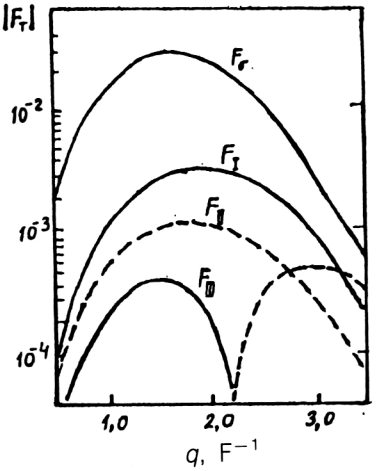

FIG. 3. MEC contributions to the $M4$ form factor of the 4^-, $T=1$ state of the ^{14}C nucleus (Refs. 22 and 23). The dashed lines show the contributions with sign opposite to the sign of the spin form factor.

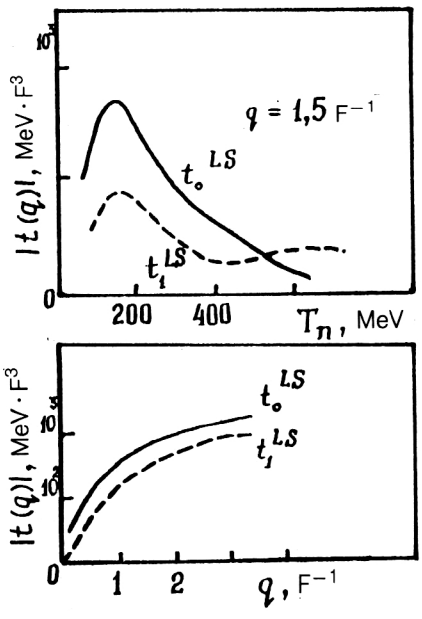

FIG. 4. Dependence of the pion–nucleon interaction amplitude on the energy and momentum transfer for transitions with parity $(-1)^{J-1}$ (Ref. 24).

Here θ is the pion scattering angle, t_T^{LS} is the effective pion–nucleon interaction amplitude responsible for MSS excitation, and a_π is the fraction of the transverse component in the relative momentum of the pion–nucleon system.[1] For transitions with change of parity $\pi=(-1)^{J-1}$, pion inelastic scattering on nuclei is dominated by the spin–orbit component of the πN interaction. In Fig. 4 we show the dependence of the isoscalar and isovector components of the effective πN interaction on the pion kinetic energy and on the momentum transfer for transitions with $\pi=(-1)^{J-1}$. For pion energies close to the Δ-isobar excitation the isoscalar component of the πN interaction t_0^{LS} dominates, and MSSs are populated mainly owing to $\Delta T=0$ processes. An important advantage of experiments using pion beams is the possibility of comparing the results obtained with negatively and positively charged pions. Such a comparison makes it possible to avoid difficulties in the definition of the absolute values of the coefficients in Eq. (31) and to determine the spectroscopic amplitudes from the ratio of the cross sections for the $(\pi^+,\pi^{+\prime})$ and $(\pi^-,\pi^{-\prime})$ reactions:

$$\frac{\sigma(\pi^+,\pi^{+\prime})}{\sigma(\pi^-,\pi^{-\prime})}=R=N\frac{(\alpha\mathscr{Z}_0-\mathscr{Z}_1)^2}{(\alpha\mathscr{Z}_0+\mathscr{Z}_1)^2}, \tag{32}$$

where the coefficient N reflects the charge dependence of the distorted pion waves. The ratio of the isoscalar and isovector components of the spin–orbit πN-interaction amplitudes is determined by the coefficient α:

$$\alpha=t_0^{LS}/t_1^{LS}. \tag{33}$$

At the energy of the pion beams at the LAMPF meson factory, $T_\pi=164$ MeV and $\alpha=1.93$ (Ref. 24). The ratio (32) makes it possible to determine the range of variation of the spectroscopic amplitudes. For this the cross-section ratio R (32) has been measured near the peak of the angular dependence of the cross section (31). For pion kinetic energies in the range 160–180 MeV the maximum of the (π,π') cross section is reached at pion scattering angles of about 70°. Equation (32) for the ratio of the spectroscopic amplitudes has two solutions:

$$\frac{\mathscr{Z}_0}{\mathscr{Z}_1}=-\frac{2}{\alpha}\frac{(R_c+1)\pm2\sqrt{R_c}}{2(R_c-1)}, \tag{34}$$

where $R_c=R/N$. The calculations in the distorted-wave impulse approximation show that for p-shell nuclei N differs from unity by 10–15%. For example, for 4^- states in ^{14}C at the peak in the angular distribution of the pion scattering cross sections at $\theta=68°$, we have $N\cong1.11$ (Ref. 25).

A choice between the two solutions for the amplitude ratio can be made by comparing the results of the calculations for (π,π') scattering with the data obtained in (e,e') experiments for the same cross-section maximum corresponding to $MJ_{\max}$ excitation of the nucleus. Therefore, MSSs offer the unique possibility of experimentally determining the spectroscopic amplitudes in a nearly model-independent fashion. It is sometimes convenient to determine not the isospin components of the spectroscopic amplitudes, but the proton and neutron components linearly related to them. These possibilities become clear in analyzing the energy dependence of the charge asymmetry of the cross sections:

$$A(\pi)=\frac{\sigma(\pi^-)-\sigma(\pi^+)}{\sigma(\pi^-)+\sigma(\pi^+)}. \tag{35}$$

In the Δ-isobar region the ratio of the pion–nucleon scattering amplitudes is

$$\left|\frac{t_{\pi^-n}}{t_{\pi^+n}}\right|=\left|\frac{t_{\pi^+p}}{t_{\pi^-p}}\right|\cong3, \tag{36}$$

so for neutrons $A(\pi)=0.8$ and for protons $A(\pi)=-0.8$.

This analysis, which was first carried out for the lowest-energy MSSs of ^{13}C nuclei (see Ref. 26), showed that the state $9/2^+$, $T=1/2$, $E=9.50$ MeV for this nucleus is a "neutron configuration," since for it $A(\pi)=0.83\pm0.10$.

The most suitable objects for a comparative analysis of the (e,e') and (π,π') reactions are MSSs with isospin equal to that of the ground state of the target nucleus, since they are populated both in strong isovector transitions in electron scattering and in the isoscalar transitions dominating in pion scattering. However, the increased accuracy in determining the excitation cross sections which was achieved in the late 1980s makes it possible to solve the inverse problem, i.e., to determine the contributions of amplitudes with different isospins to the MSS wave function.

The unique possibilities offered by MSSs for separating the spectroscopic characteristics from the features of the interaction dynamics of the test particle and the nucleus are also realized in the analysis of reactions induced by nucleons. For the cross sections of these reactions the re-

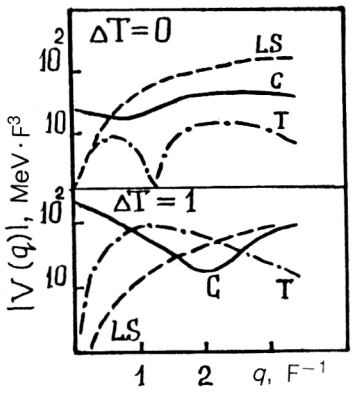

FIG. 5. Dependence of the nucleon–nucleon interaction amplitude on the momentum transfer for $E_p=135$ MeV; $\pi=(-1)^{J-1}$ (Ref. 27).

lation to the effective nucleon–nucleon interaction is more complicated than for (π,π') reactions (Refs. 1, 25, and 27):

$$\left.\frac{d\sigma}{d\Omega}\right|_{(N,N')}=\frac{1}{\pi}M_N^2\sum_{T=0,1}\{J|V_T^{\parallel}(q)|^2+(J+1)[|V_T(q)| +|V_T(q)|]^2+\tfrac{1}{2}(J+1)(k_N/q)^4\alpha_p^2 \times\sin^2\theta|V_T^{LS}(q)|^2\}|\mathscr{F}_{JT}\rho_J^s(q)|^2. \quad (37)$$

Here $V^{\parallel}(q)=V_c(q)-2V^T(q)$ and $V(q)=V_c(q)+V^T(q)$ are linear combinations of the central and tensor components of the effective nucleon–nucleon interaction and V^{LS} is its spin–orbit component. The factor α_p reflects the contribution of the longitudinal momentum in the NN system.[1,27]

The role of the different components of the NN interaction in transitions with change of parity $\Delta\pi=(-1)^{J-1}$ is shown in Fig. 5 for isoscalar and isovector excitations. For large momentum transfers q to the nucleus, the isovector excitation of MSSs in the nucleon beam is dominated by the tensor component of the NN interaction near the maximum of the spin transition density for $MJ_{\max}$ transitions. Increase of the momentum transfer increases the contribution of the spin–orbit component of the interaction, which dominates in isoscalar excitations. Comparison of the results from (e,e') and (p,p') reactions [and also the (p,n) reaction] is an interesting way of studying the tensor component of the effective NN interaction, since, according to microscopic calculations, tensor forces arise owing to the exchange of a single pion at small momentum transfers and owing to ρ-meson exchange at large q. The discovery of contributions from other graphs to the tensor component and a deeper understanding of the role of meson exchange and quark–gluon effects at large momentum transfers are problems in whose solution the study of MSSs with various test particles can prove decisive.

The most complete analysis of the MSS excitation cross sections has been carried out for the ^{16}O (4^-, $T=1$, $E=18.98$ MeV; see Fig. 6) and ^{28}Si (6^-, $T=1$, $E=14.36$ MeV; see Fig. 7) nuclei in a series of (e,e'), $(\pi^+,\pi^{+\prime})$, $(\pi^-,\pi^{-\prime})$, (p,p'), and (p,n) experiments (Refs. 28–31, 11, 9, and 32). Study of these results leads to the following conclusions:

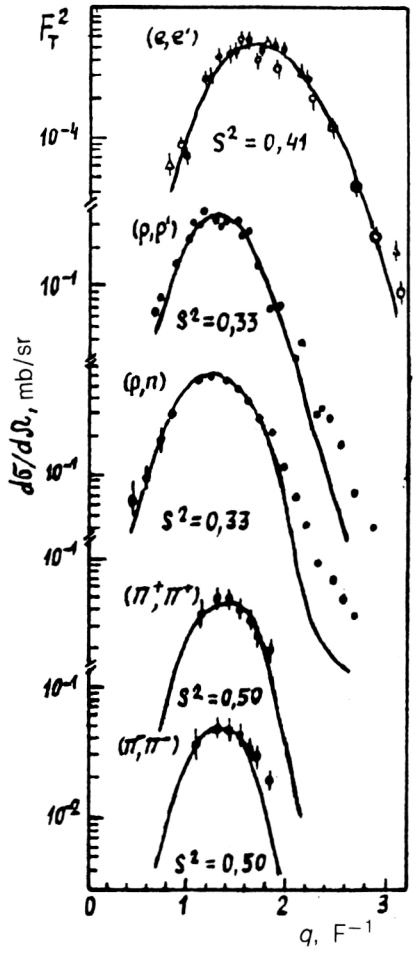

FIG. 6. Excitation cross sections of the 4^-, $T=1$, $E=18.98$ MeV state of the ^{16}O nucleus. The solid lines are the result of calculations using the particle–hole model for the $|p_{3/2}^{-1}d_{5/2}:4^-\rangle$ configuration (Ref. 1).

1) The assumption that the cross section is dominated by both electromagnetic and hadronic MSS excitations of the purely spin transition density corresponds to the experimental picture.

2) The momentum-transfer dependence of the hadron excitation cross sections is realistically reproduced by the calculations using the DWIA (distorted-wave impulse approximation).

3) The suppression factors for $MJ_{\max}$ transitions obtained by comparing the experimental data with calculations using the particle–hole model agree to within 20%. This is illustrated in Table I.

The difference between the S^2 factors for electron and hadron MSS excitation reactions are largest for protons, which reflects the level of reliability of the model approximations for the proton–nucleus interaction amplitudes. However, the agreement (to within 20%) of the S^2 factors at the same time suggests that the MSS suppression is related to the structure of the nucleus or, more precisely, to the unrealistic treatment of the ground and excited states

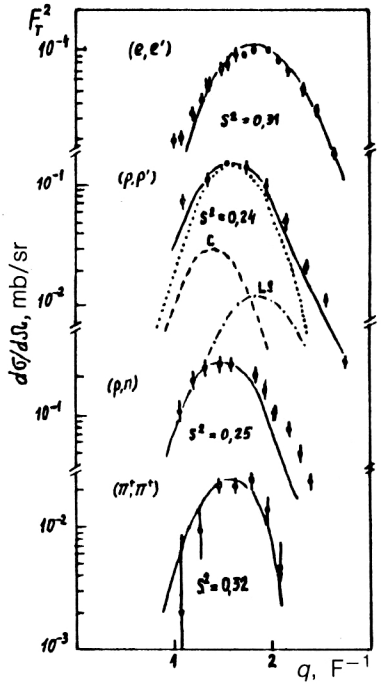

FIG. 7. Distribution of experimental and theoretical cross sections for $M6$ excitations of the ^{28}Si nucleus (Ref. 1).

in the limiting particle–hole model. The above summary of the inclusion of the MEC effect on the MSS suppression indicates that more attention must be paid to the problem of the nuclear wave functions. It should be emphasized that studies of suppressions of isoscalar $MJ_{\max}$ transitions carried out in hadron beams have finally eliminated the possibility of attributing the suppression to the effect of excitations of states of the $\Delta-h$ type, i.e., transfers of part of the $MJ_{\max}$ transition strength to higher excitation energies in the Δ-isobar range. The point is that the suppression of isoscalar states of maximum spin turned out to be even stronger than the suppression of isovector ones. Measurements of the cross sections for (p,p') and $(\pi^{\pm},\pi^{\pm\prime})$ reactions on the ^{28}Si nucleus have shown (see Ref. 26) that for the 6^-, $T=0$, $E=11.577$ MeV level the S^2 factor is about 0.12, i.e., half that for the 6^-, $T=1$, $E=14.36$ MeV state.

The theoretical overestimate of the multipole excitation strengths compared with the experimentally observed MGR strength is a typical feature of nuclear models which attempt a microscopic description of excited nuclear states. The suppression problem was discussed in Ref. 42 in connection with calculations of the strengths of nuclear excitations of lowest multipole order. In our opinion, the route to a solution of this problem lies in the detailed analysis of the possibilities offered by microscopic models for states of the simplest structure like MSSs.

One of the acknowledged sources of suppression of the multipole excitation strengths is the damping related to the interaction of the doorway configurations with more complicated configurations in the nucleus, primarily with collective phonons. However, a difficulty arises in attempting to find the degree to which such configurations are coupled. This is that for most multipole excitations it is impossible to separate the factors responsible for the mixing of the doorway configurations themselves from the factors for the mixing of configurations of a different degree of complexity. In other words, the relative contribution of one-phonon, two-phonon, etc., configurations is usually estimated phenomenologically. MSSs are distinguished from other MGRs by the extreme simplicity of the doorway excitation. For even nuclei the doorway MSS configuration is a particle–hole pair with a given isospin. Since mixing is absent at this level of excitation, the actual MSS fragmentation is a consequence, first, of the features of the structure of the ground state of the target nucleus and, second, of the interaction of the doorway configuration with more complicated states. These two factors can be understood by studying MSSs. As seen from comparison of the (e,e') and (π,π') cross sections, the study of MSSs with various test particles makes it possible to obtain not only the multipole excitation strength, but also the value of the spectroscopic amplitude. Therefore, MSSs permit us to go to the next stage in the microscopic study of the wave functions of nuclear states. For example, significant progress has been achieved in understanding isospin mixing by studying the 4^- states of the ^{12}O and ^{12}C nuclei (Refs. 33, 28, and 66). At present, MSSs provide the most critical test of microscopic methods of describing nuclear excitations.

The methods described above for comparative analysis of the data of electron and hadron experiments are most

TABLE I. MSS suppression factors in reactions involving electrons and hadrons (Ref. 20).

Nucleus	Reaction	E, MeV	J^π, T	S^2	$S^2(h,h')/S^2(e,e')$
^{16}O	(p,p')	18,98	4^-, 1	0,33	0,81±0,04
^{16}O	$(\pi^+,\pi^{+\prime})$	–"–	–"–	0,50	1,22±0,06
^{16}O	$(\pi^-,\pi^{-\prime})$	–"–	–"–	0,50	1,22±0,06
^{28}Si	(p,p)	14,36	6^-, 1	0,24	0,88±0,06
^{28}Si	(p,n)	–"–	–"–	0,25	0,81±0,03
^{28}Si	$(\pi^+,\pi^{+\prime})$	–"–	–"–	0,32	1,03±0,03
^{28}Si	$(\pi^-,\pi^{-\prime})$	–"–	–"–	0,32	1,03±0,03

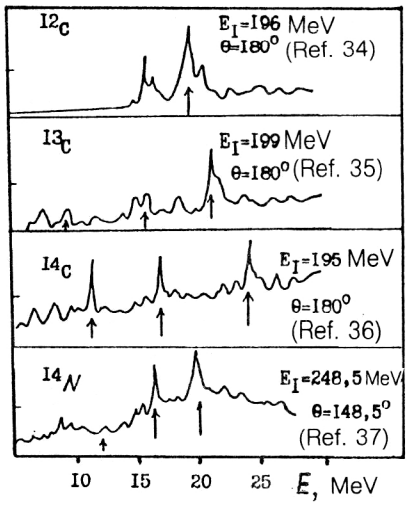

FIG. 8. Cross sections for large-angle electron scattering for the ^{12}C, ^{13}C, ^{14}C, and ^{15}N nuclei (Refs. 34–37). The arrows indicate the states arising in $M4$ transitions.

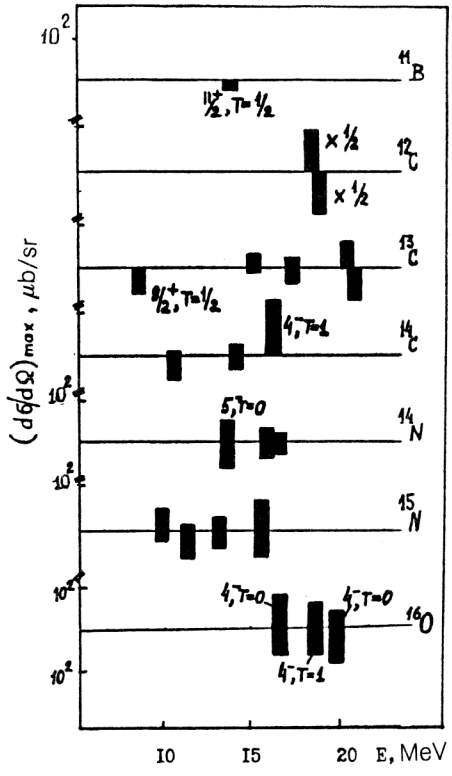

FIG. 9. $M4$ excitations in the cross sections for pion scattering on p-shell nuclei. The cross sections for positive pions are given above the intersection of the axes, and those for negative pions are given below (Refs. 26 and 38).

successfully realized for p-shell nuclei. For intermediate and heavy nuclei the identification of peaks in hadron scattering at high (above 10 MeV) excitation energies runs into great difficulties, but for light nuclei this identification has been done for many even nuclei and a few odd ones. Naturally, the simplest spectra are those of excited nuclei with $J_0=0$, when the $M4$ excitation leads to states with $J_f=4^-$. This has been done for the ^{12}C, ^{14}C, and ^{16}O nuclei, for which data from a comparative analysis of (e,e') and $(\pi^{\pm},\pi^{\pm\prime})$ experiments are available for excitation energies $E<25$ MeV. The excitation spectrum of the ^{14}N nucleus is considerably more complicated. Here $M4$ transitions excite three spin branches of states with $J_f=3^-$, 4^-, and 5^-. For odd nuclei the excitation picture is made up of the excitation spectra of the $9/2^+$ and $7/2^+$ states for nuclei with $J_0=1/2^-$ and the $11/2^+$, $9/2^+$, $7/2^+$, and $5/2^+$ states for nuclei with $J_0=3/2^-$. Isovector $M4$ excitations, which dominate in inelastic (e,e') scattering, give a single isospin branch $T_0=1$ only in the case of nuclei with $T_0=0$ (^{12}C, ^{14}N, and ^{16}O). For the other p-shell nuclei studied, two isospin branches $T_<$ and $T_>$ are involved in the isovector excitations.

In Fig. 8 we show the energy dependences of the effective cross sections of (e,e') reactions on ^{12}C (Ref. 34), ^{13}C (Ref. 35), ^{14}C (Ref. 36), and ^{14}N (Ref. 37) nuclei obtained at the values of the momentum transfer for which the form factors of $M4$ transitions are close to the maximum. All the experiments except the ^{14}N (e,e') one were carried out at the BATES MIT accelerator at the electron scattering angle 180°, which ensures that contributions from longitudinal form factors are absent in the nuclear-excitation cross section.

During the last ten years a series of experiments have been carried out at the LAMPF meson factory to study the effective nuclear-excitation cross sections in the inelastic scattering of positive and negative pions at kinetic energies corresponding to the Δ resonance in the πN interaction. A strength of these experiments is the reliable separation of transitions with $\Delta S=0$ and ones with $\Delta S=1$, which was achieved using the behavior of the effective excitation cross section of the peak in question as a function of the pion energy for fixed momentum transferred to the nucleus. Since $q^2\cong 2k_\pi^2(1-\cos\theta)$, the growth of T_π and k_π for fixed q is accompanied by growth of $\cos\theta$ and decrease of $\sin\theta$. This leads to a decrease of the contribution of the nucleon-spin-flipping component of the pion–nucleon interaction:[39]

$$f_{\pi N}=\alpha(k)(2\cos\theta'+i\vec{\sigma}\vec{n}\sin\theta'), \qquad (38)$$

where $\alpha(k)$ reflects the energy dependence of the elementary amplitude, θ' is the scattering angle in the c.m. frame, and $\vec{n}$ is the normal to the πN scattering plane. The second term in (38), related to the spin–orbit strengths of the πN interaction, induces transitions with $\Delta S=1$, including $M4$ excitations in p-shell nuclei.

In Fig. 9 we schematically show the results of studying $M4$ transitions in p-shell nuclei at the LAMPF pion beams.[26,38]

The experimental data shown in Fig. 9 for the contribution of $M4$ transitions to the cross section for the scattering of positive (upper scale) and negative (lower scale) pions on p-shell nuclei are most reliable at low excitation energies, when the density of states is not very large. At present, MSSs at $E=21.47$ MeV have only been identified in the ^{13}C nucleus; the multipole analysis of scattering at

large momentum transfers has not yet been performed for other nuclei at these and higher energies. The difficulty of this analysis is enhanced by the presence of a large number of peaks of various multipole orders in this energy range at momentum transfers of ~ 1.7 F^{-1}. The possibilities of a microscopic approach to the multipole analysis of particular cross sections will be discussed below. The results of experimental (e,e') and (π,π') studies of p-shell nuclei reveal the main feature of the distribution of $M4$-transition strengths: the action of the same operator $j_3(qr)[Y_3\times\sigma]_4$ on the wave function of the nuclear ground state leads to greatly different $M4$-transition strength distributions for different p-shell nuclei.

The following sections of this review will be devoted to discussion of possible interpretations of the $M4$-resonance characteristics on the basis of the multiparticle shell model. We shall consider nuclei with a p shell which is not closed from the viewpoint of the limiting model. The interpretation of the structure of the MGR in the ^{16}O nucleus requires deeper understanding of the role of complicated configurations of the type $2p2h$, $4p4h$, etc., in the functions describing the nuclear response to excitation and is a separate problem in nuclear theory.

2. MICROSCOPIC DESCRIPTION OF $M4$ EXCITATIONS OF p-SHELL NUCLEI

The new experimental possibilities for studying multipole resonances in the effective cross sections have made it imperative to interpret the differential characteristics of nuclear excitations. The new emphasis on exclusive experiments, the complex studies of the nuclear response to excitation by various test particles, and the discovery of fine structure in the nuclear excitation spectra are stimulating the development of microscopic and semimicroscopic methods of describing nuclear states. It has become necessary to extend the quantum field techniques used in nuclear theory to nuclei whose ground state does not correspond to a closed shell or subshell. This problem is particularly acute for light nuclei, for which the nuclear reaction cross sections clearly manifest the individual characteristics of the nucleon systems. The methods of describing nuclear multipole excitations based on the multiparticle shell model have performed fairly well in studies of the structure and properties of the electric dipole resonance in the photodisintegration cross sections. The results of experimental and theoretical studies of the $E1$ resonance in p-shell nuclei are reviewed in Refs. 40–42. The increased momentum transfer to the nucleus in the experiments makes it necessary for the theoretical models to describe nuclear excitations of different multipole orders in a unified manner.

For p-shell nuclei $1\hbar\omega$ multipole resonances are described microscopically by using two versions of the multiparticle shell model. In one the wave functions of excited states with parity opposite to that of the ground state of the target nucleus are constructed as linear combinations of products of wave functions of nucleon configurations (see Refs. 41–45, for example).

Another version of the representation of the excited-state wave functions is their decomposition in the set of basis configurations of the particle plus nuclear final state (PNFS; Refs. 46, 41, and 42):

$$|J_fR_f\alpha_f\rangle=\sum_{j',(J'T'E')}\beta_f^{(J'T'E'),j'}|(J'T'E')\times(n'l'j'):J_fT_f\alpha_f\rangle. \tag{39}$$

Here $|J'T'E'\rangle$ is the state of the nucleus with $A-1$ nucleons, and $|n'l'j'\rangle$ is the nucleon state. For $1\hbar\omega$ excitations of p-shell nuclei the basis (39) is constructed by using the wave functions of the nucleons in the $1d$–$2s$ shell. In other words, the basis configurations of the problem of excited states correspond to the configurations arising in transitions of a nucleon from the ground state to the next shell:

$$|(J'T'E')\times(j'):J_fT_f\rangle=\sum_{j,J}\gamma^j[a_{j'}^+\times a_j]_J|J_0T_0\rangle. \tag{40}$$

This treatment of the wave function of the excited nucleus is obviously unrelated to the problem of closed shells or subshells in the ground state and corresponds to the decomposition of hole configurations in real states of the nucleus $A-1$:

$$a_j|J_0T_0\rangle=\sum_{(J'T'E')}\delta^{j,(J'T'E')}|J'T'E'\rangle. \tag{41}$$

The set of PNFS basis configurations is in principle a complete set and can be expanded in the complete set of nucleon multiparticle configurations. The advantages of the PNFS system are manifested in the fact that, owing to the representation of $(A-1)$-nucleon configurations in the form of real states of the nucleus $A-1$, a physically justified truncation of the basis becomes possible. If the nuclear excitation arises owing to a single interaction of the incident particle with the system of nucleons, the matrix elements of the excitation operator B_{JM_J} will play the leading role in the excitation functions. In the PNFS basis the matrix elements of the operator (17) have the form ($\hat{a}=\sqrt{2a+1}$)

$$\begin{aligned}\langle J_fM_{T_f}T_f\alpha_f\|\hat{B}_J\|J_iT_iM_{T_i}\alpha_i\rangle&=\sum_{i,j_fj_i}\langle j_f\|\hat{O}_J\|j_i\rangle\sqrt{2}\hat{J}_i\hat{T}\hat{T}_i\hat{J}_f\langle T_iM_{T_i}T0|T_fM_{T_f}\rangle n\\&\times\sum_{J'T'E'}\langle J_fT_f\alpha_f|(J'T'E'),j_f\rangle\langle(J'T'E'),j_i\\&\times|J_iT_i\alpha_i\rangle(-1)^{J'-J_i-J+j_f+T'-T_i-T+1/2}\\&\times W(J_iJ_fj_ij_f;JJ')W(T_iT_f1/2\ 1/2;TT'),\end{aligned} \tag{42}$$

where the spectroscopic amplitude of the multipole excitation is

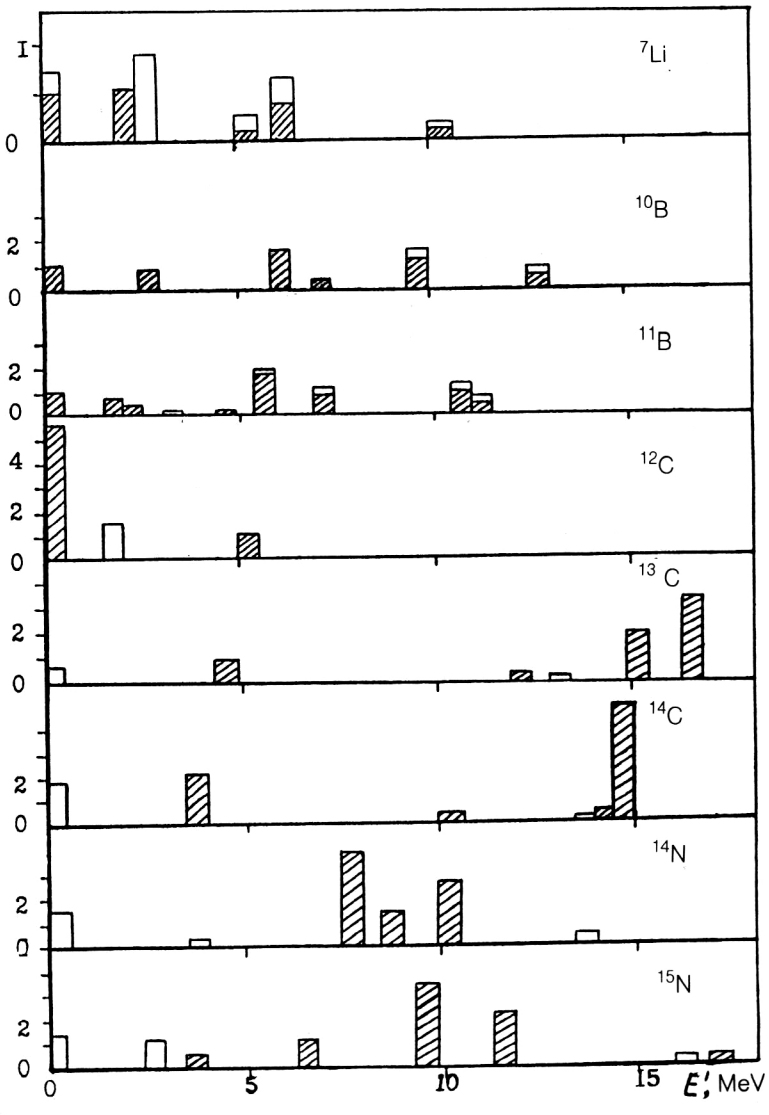

FIG. 10. Distributions of the spectroscopic factor for removal of a p nucleon (Ref. 48). The contributions of $p_{3/2}$ nucleons are shaded.

$$\mathscr{Z}_{J,TM_T}(j_f j_i) = \sqrt{(2T+1)(2T+1)(2J_f+1)}\langle T_i M_{T_i} T M_T | T_f M_{T_f}\rangle n \times \sum_{J'T'E'} \langle J_f T_f \alpha_f | (J'T'E'), j_f\rangle \langle (J'T'E'), j_i \times |J_i T_i \alpha_i\rangle (-1)^{J'-J_i+j_f-J+T'-T_i-T+1/2} \times W(J_i J_f j_i j_f; JJ') W(T_i T_f 1/2\ 1/2; TT'). \quad (43)$$

If $|J_i T_i \alpha_i\rangle$ is the ground state of the target nucleus, then the nonzero matrix elements in (42) are those which include states of the final nucleus $|J'T'E'\rangle$ having a direct parentage relation to the ground state:

$$|J_0 T_0\rangle = \sum_{(J'T'E'),j} C_0^{J',j} |(J'T'E') \times (nlj): J_0 T_0\rangle. \quad (44)$$

Here $C^{J',j}$ is the single-nucleon parentage coefficient.

The wave functions of the ground and lowest excited states of p-shell nuclei obtained in Refs. 47 and 48 correspond to the distribution of the ground-state spectroscopic factors shown in Fig. 10. The study of the ^{12}C nucleus in the $(e,e'p)$ reaction at electron energies 280–480 MeV carried out at the NIKHEF accelerator[49] showed that the discrepancy between the spectroscopic factors of Ref. 48 and the experimental data for ^{12}C is less than 15% for transitions to the states $|3/2^-,\ T=1/2;\ E=0\rangle$, $|3/2^-,\ T=1/2;\ E=5.02$ MeV$\rangle$, and $|1/2^-,\ T=1/2;\ E=2.12$ MeV$\rangle$ for the ^{11}B nucleus.

From the structure of the matrix elements of the excitation operators (42) it follows that in solving the problem of $1\hbar\omega$ excitations of nuclei using the PNFS basis it is necessary to include in the final-nucleus configurations $|J'T'E'\rangle$ all states with nonzero parentage coefficient relative to the ground state of the target nucleus. This truncation of the full basis corresponds to including only doorway configurations in the calculation. Numerous specific MGR calculations have shown that in a first approximation, $1\hbar\omega$ multipole excitations of nuclei correspond to "semidirect" processes in a system of A nucleons, when the formation of the structure of the excitation functions is dominated by the interaction of doorway configurations.

The PNFS approach has the following advantages over

TABLE II. Dimension of the space of $1\hbar\omega$ multipole excitations of p-shell nuclei. The first column is for the PNFS basis, and the second is for the complete nucleon-configuration basis (Ref. 45).

A_X	T_f	J_f^π, even nuclei															
		0^-		1^-		2^-		3^-		4^-		5^-		6^-		7^-	
^{6}Li	1	2	8	5	19	5	18	3	10	1	3						
^{8}Be	1	8	32	27	81	24	91	15	68	5	35		11		2		
^{10}Be	1	7	62	19	160	27	190	28	157	23	96	14	42	6	13	2	2
^{12}C	1	3	55	8	141	8	167	5	139	2	87		40		13		2
^{14}C	1	9	20	23	50	23	56	14	43	8	24		9		2		
^{14}N	1	9		21		25		18		9		3					
^{14}C	2	3	5	8	13	8	14	5	10	2	5		1				
^{16}O	1	2	2	5	5	5	5	3	3	1	1						

A_X	T_f	J_f^π, odd nuclei											
		$1/2^+$		$3/2^+$		$5/2^+$		$7/2^+$		$9/2^+$		$11/2^+$	
^{7}Li	1/2	14	36	21	52	19	45	15	26	5	9	1	1
	3/2	7	21	10	29	9	24	8	11	2	3		
^{9}Be	1/2	28	97	47	148	44	146	33	102	17	51	6	17
	3/2	16	66	28	99	25	91	18	57	9	26	3	7
^{11}B	1/2	40	125	61	197	55	199	40	147	19	83	6	34
	3/2	22	89	34	136	32	131	24	89	12	46	4	16
^{13}C	1/2	28	75	40	115	30	112	18	79	6	43		11
	3/2	14	48	20	75	15	68	9	45	3	22		7
^{15}N	1/2	16	18	23	25	19	22	10	13	3	5		1
	3/2	8	8	11	11	10	10	5	5	2	2		

the version of the multiparticle shell model based on multinucleon configurations.

For complex nuclei the number of basis states in the problem of MGR excitations in the PNFS approach is considerably smaller than in the nucleon-configuration basis. This is illustrated in Table II. It should be noted that this advantage of the PNFS approach, which makes it possible, for example, to use it to solve the problem of dipole excitations of nuclei at the center of the p shell,[50,51] is not so important for high-spin excitations, when the size of the basis is small in both versions of the shell model.

Apparently, a more important advantage of the PNFS approach is the relative simplicity of the procedure for calculating the MGR decay characteristics for nucleon decay channels.

Finally, the energy dependence of the MGR excitation cross sections is reproduced in the PNFS version more realistically than in other versions of the shell model. This difference is clearest for nuclei with a complicated parentage structure, for example, for nuclei of the center of the p shell, ^{10}B and ^{11}B. In the PNFS approach the structure of the excitation functions of these nuclei is more complicated, and the transition strength is distributed over a wider range of excitation energies than in other versions of microscopic models (see Refs. 41 and 42).

This latter feature of the calculations of the MGR cross sections using the PNFS approach is a consequence of the direct inclusion of the excitation energies of the final nuclei $A-1$ in the diagonal matrix elements of the Hamiltonian:

$$\langle (J'T'E')(n'l'j'):J_fT_f|\hat{H}|(J'T'E')(n'l'j'):J_fT_f\rangle$$

$$=E'+E_b+\varepsilon_{j'}-E_c+\langle (J'T'E')\times(n'l'j'):J_fT_f|\hat{V}|(J'T'E')(n'l'j'):J_fT_f\rangle. \quad (45)$$

Here $\varepsilon_{j'}$ is the nucleon energy in the state $|n'l'j'\rangle$; E_b is the binding energy of the nucleon in the nucleus A; E' is the excitation energy of the level $|(J'T'E')\rangle$ in the nucleus $A-1$; $\langle|V|\rangle$ is the diagonal element of the residual nucleon–nucleus interaction; E_c is an energy parameter reflecting the interaction of the nucleon with the nucleus A. The last of these quantities in general depends on the nucleon state. For the ^{12}C nucleus this parameter can be calculated and is about 6 MeV. In calculations of p-shell nuclei from ^{7}Li to ^{15}N, E_c is a phenomenological parameter differing from nucleus to nucleus, but the same for all excited states of a given nucleus A. Its value is determined from the position of the lowest energy levels of the nucleus A for states with parity opposite to that of the ground state.

For nuclei with complex parentage structure of the ground states, the matrix elements of the Hamiltonian (45) have an energy spread which on the average is close to the energy range of the states of the final nucleus $A-1$ which are coupled to the ground state of the target nucleus. In other words, the distribution shown in Fig. 10 affects the MGR energy distribution.

The matrix elements of the residual-interaction Hamiltonian are related in the PNFS approach to the matrix

elements of the nucleon–nucleon interactions, $\langle jj_1{:}JT|\hat{V}|j'j_2{:}JT\rangle$, as

$$\langle (J'T'E')\times(n_1l_1j_1){:}J_fT_f|\hat{V}|(J''T''E'')(n_2l_2j_2){:}J_fT_f\rangle$$

$$=n\sum_{j,j'}\sum_{m,JT}\langle (J'T'E')|m,j\rangle\langle m,j'|(J''T''E'')\rangle$$
$$\times\hat{J}^2\hat{T}^2\hat{j}'\hat{T}'\hat{J}''\hat{T}''W(J_mjJ_fj_1;J'J)W$$
$$\times(J_mj'J_fj_2;J''J)W(T_m1/2T_f1/2;T'T)W$$
$$\times(T_m1/2T_f1/2;T''T)\langle jj_1{:}JT|\hat{V}|j'j_2{:}JT\rangle. \quad (46)$$

Here $\langle (J'T'E')|m,j\rangle$ and $\langle (J''T''E'')|m,j'\rangle$ are the parentage coefficients for the removal of a nucleon from the nucleus $A-1$ in the states $|J'T'E'\rangle$ and $|J''T''E''\rangle$, n is the number of nucleons in the shell, and $\hat{a}=\sqrt{2a+1}$.

The nucleon–nucleon interaction potential can be written as the sum of central, spin–orbit, and tensor parts:

$$\hat{V}(r)=\hat{V}^C(r)+\hat{V}^{LS}(r)+\hat{V}^T(r). \quad (47)$$

In the calculations (Refs. 41–46 and 50–59) of the MGR of p-shell nuclei a purely central residual-interaction potential was used,

$$\hat{V}^C(r)=\hat{V}_0^Cf^C(r)\sum_{T,S=0,1}a_{TS}^{TS}P, \quad (48)$$

and the mixing parameters in most of the calculations were chosen as in Ref. 60. The depth of the potential well was 45 MeV; for $f^C(r)$ a Gaussian form of the potential well, $\exp(-r^2/\mu^2)$, was used; the ratio of the well parameter to the oscillator parameter of the nucleon wave functions was 1.03 (see the review of Ref. 42). The effect of the residual-interaction parameters on the distribution of MGR cross sections has been studied for the ^{15}N nucleus.[56]

The theoretical calculations of Refs. 22, 25, 34, and 38 also included the tensor term in the residual-interaction potential (47).

The wave functions of nuclear excited states obtained by diagonalizing the Hamiltonian $\hat{H}$ on the PNFS basis contain an admixture of "false" states corresponding to motion of the nuclear center of mass. These states are isolated by constructing the wave functions of the false states and then orthogonalizing the basis relative to them.

The microscopic description of $1\hbar\omega$ excitations based on the use of the parentage structure of the ground state of the target nucleus, i.e., the PNFS approach, is usually not involved in the calculation of deep hole states of the target nucleus. The process of nucleon knockout from deep shells, for example, the $1s$ shell in the case of the excitation of p-shell nuclei, leads, as a rule, either to direct decay of the nucleus via cluster channels or to the formation of a product nucleus in highly excited states, the typical energies of which are considerably higher than the MGR localization region corresponding to the transition from the p shell. However, for nuclei at the beginning and middle of the p shell the regions of the transitions $1s\rightarrow 1p$ and $1p\rightarrow(1d,2s)$ overlap for multipole resonances of lowest spin. This difficulty is absent for states of maximum spin, where transitions from deep shells do not play any role in the formation of the $M4$ excitation cross sections.

Restriction of the basis (39) to only those states of the final nucleus $|J'T'E'\rangle$ which have a direct parentage connection to the ground state of the target nucleus $|J_0T_0\rangle$ is the "minimal" PNFS approximation. The approach admits expansion of the basis by including in it those states of the nucleus $A-1$ which have parentage connection to the collective lowest excitations of the target nucleus. For example, for the ^{12}C nucleus, which was the first object to which the PNFS scheme was applied,[46,53] it is natural to extend the basis by including those states of the nuclei ^{11}C–^{11}B which are related to the first 2^+, $T=0$ excited state of the ^{12}C nucleus. This implies the inclusion of not only the $3/2_1$, $3/2_2$, and $1/2_1$ states but also the $5/2_1$, $5/2_2$, and $7/2_1$ states of the product nuclei in the configurations of nuclei with $A=11$. This method of including the interaction of doorway states with collective excitations of the target nucleus does not violate the Pauli principle. The effectiveness of this method of expanding the basis in the problem of excited nuclear states is confirmed by the fact that by using the basis thus extended it is possible to obtain an adequate description of the $E1$ resonance above the first excited state of the ^{12}C nucleus, the structure of whose excitation cross section corresponds to the experimental data on the ^{11}B$(p,\gamma_2)^{12}$C reaction.[57,61]

The results of theoretical calculations of $M4$ excitations of the ^{11}B, ^{12}C, ^{13}C, ^{14}C, ^{14}N, and ^{15}N nuclei carried out using the PNFS approach to the multiparticle shell model are shown in Fig. 11 (Ref. 58). The transverse form factors of electron inelastic scattering are shown for momentum transfer to the nucleus corresponding to the maximum of the $M4$ form factor, i.e., for 1.7 F^{-1}. Experimental information on the $M4$ cross sections is available for all the nuclei shown in Fig. 11, although for some of them, for example, ^{11}B, $M4$-excitation peaks have been identified only at low energies, while excitation energies above 20 MeV have essentially not been studied. In Figs. 12 and 13 we show the results of the PNFS calculations for the ^{7}Li and ^{10}B nuclei (Refs. 59 and 62). Of these nuclei, only for ^{10}B are there preliminary data on the ^{10}B(π,π') and ^{10}B(p,p') cross sections, but the excitation energy in these reactions is still too small for $M4$ peaks of the cross sections to be discovered.[64] In all the figures we give the values of the transverse form factor $F_T^2(q)$ on a logarithmic scale, which allows the complicated structure of the excitation function to be seen.

Let us consider some general characteristics of $M4$ excitations in p-shell nuclei. All the maxima of the $M4$ cross sections shown in Figs. 11–13 are the result of the fragmentation of the strength of a single doorway particle–hole excitation $p_{3/2}^{-1}d_{5/2}$ and its interaction with the core. Since for the states of maximum spin excited in $M4$ transitions the mixing of doorway configurations and collectivization of states plays a smaller role than for states of lowest spin of the excitation, the effect of the distribution of the parentage coefficients among the states of the final nuclei is manifested more clearly for them. Comparison of Fig. 10

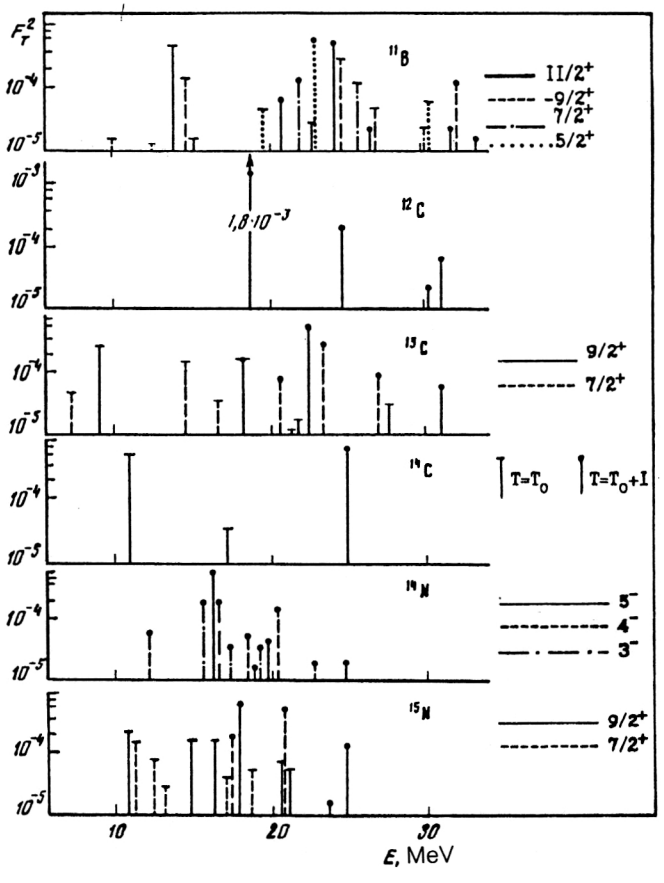

FIG. 11. Distribution of the form factors of $M4$ excitations in the nuclei ^{11}B, ^{12}C, ^{13}C, ^{14}N, and ^{15}N (Ref. 58) for $q=1.7$ F^{-1}.

for the distribution of the spectroscopic factor $S(p_{3/2})$ with the result of the calculation in Figs. 11–13 and the experimental distributions of the (e,e') and (π,π') cross sections (Figs. 8 and 9) shows that an important role is played by the energy spread of the hole over final nuclear states in the formation of the energy distribution of the $M4$-excitation cross sections. The second factor determining the structure is the isospin splitting of groups of states with $T=T_<$ and $T_>$ for non-self-conjugate nuclei. The energy spread of the $T_<$ states is considerably broader than for $T_>$ states. The region of low excitation energies is formed practically only by $T_<$ states, but the region of excitation energies above 18 MeV, where the peaks of the cross sections with $T=T_>$ are concentrated, also contains a significant fraction of strengths of MSSs with $T=T_<$.

The exception is the ^{14}C nucleus, for which only 1% of the strength of the 4^-, $T=1$ states lies above 18 MeV, according to the PNFS calculation.

The states of lowest energy with maximum spin $J=J_0+4$ in nuclei with $T_0\neq0$ are states with $T=T_0$, whose wave function is dominated by configurations constructed from the lowest-energy states of the nucleus $A-1$. In Table III we list these states and give the configurations which dominate in their wave functions. We see from this table that the lowest-energy MSSs of the ^{11}B, ^{13}C, and ^{7}Li nuclei are neutron–core configurations, so that they must be excited primarily in $(\pi^-,\pi^{-\prime})$ reactions. For the nuclei ^{13}C and ^{11}B this corresponds to the experimental data of Ref. 26. The $M4$ excitations of the ^{7}Li nucleus have not yet been studied. The situation regarding the lowest-energy $9/2^+$ state of ^{15}N is more complicated. In the isospin representation, the wave function of this state is dominated by the configuration corresponding to the sum of proton and neutron configurations above the isobar-analog 2^+, $T=1$ states in ^{14}C and ^{14}N, where the contributions of proton and neutron configurations have identical amplitudes. The calculation in the proton–neutron representation doubles the dimension of the Hamiltonian matrix compared with the isospin representation and simultaneously leads to a more realistic picture of the amplitude distribution: configurations constructed on the lowest-energy state of the core plus nucleus with $A=14$ begin to dominate. The state $|2^+, T=1; E=7.01$ MeV$\rangle$ of the ^{14}C nucleus is such a state in this case. In other words, the inclusion of the actual excitation energies of the analog states of the final nuclei leads to the conclusion that the lowest-energy MSS of the ^{15}N nucleus must predominantly be excited in inelastic $(\pi^+,\pi^{+\prime})$ scattering reactions. This is corroborated by the experimental picture of the ratio of $\sigma(\pi^+,\pi^{+\prime})$ and $\sigma(\pi^-,\pi^{-\prime})$ shown in Fig. 9 (Ref. 38).

In analyzing the experimental cross sections for (e,e') and (π,π') reactions it is necessary to include the possibil-

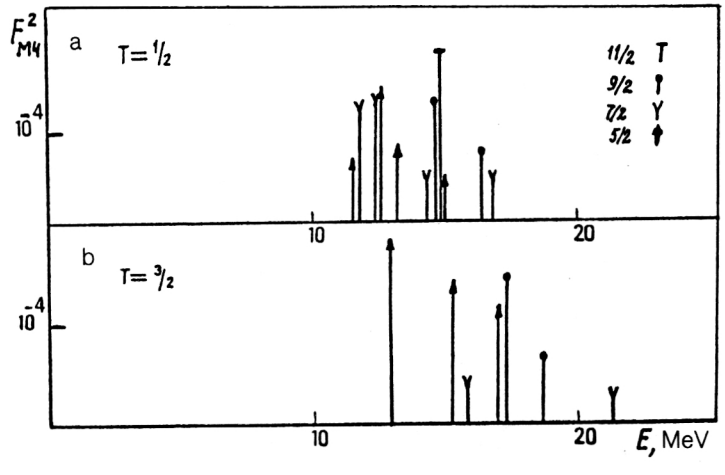

FIG. 12. $M4$ excitations of the nucleus ^{7}Li. Form factors F_T^2 for $q=1.7$ F^{-1} (Ref. 59).

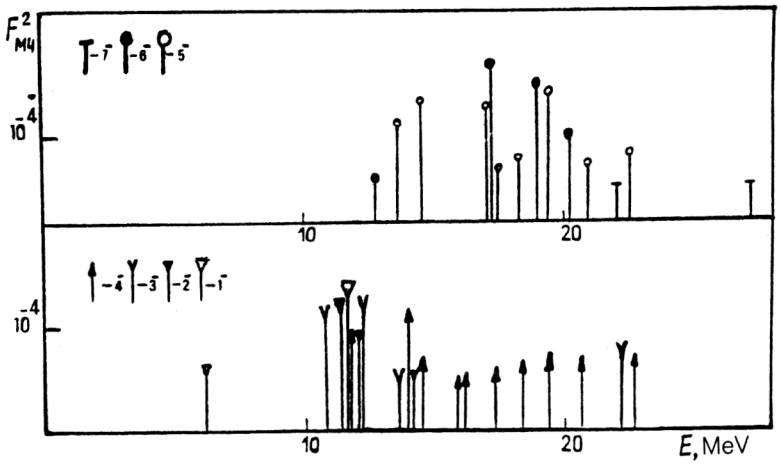

FIG. 13. Form factors of the $M4$ excitation of the nucleus ^{10}B for $q=1.7$ F^{-1} (Ref. 62).

ity for nuclei with $J_0 \neq 0$ of populating the same states not only in the $M4$ excitation process, but also in transitions of lower multipole order. The situation is also complicated by the fact that the momentum-transfer dependence of the $M4$-transition form factor, which reaches a maximum for $q=1.7$–1.8 F^{-1}, is similar to the q dependence of the transverse form factor of the $E3$ excitation, which can give a large contribution to the population of states with $J<J_0+4$. In this region of momentum transfers, $q>1.5$ F^{-1}, spin-octupole $M2$-excitation modes give a significant contribution to the excitation cross section. It is significant that the location of the extremum of the multipole form factor at which the contribution of the spin-multipole operator $[Y_3 \times \vec{\sigma}]_J$ dominates for all possible multipole orders, i.e., $M2$, $E3$, and $M4$, is practically independent of the spin of the transition. This follows from the q dependence of the transverse form factors of $1\hbar\omega$ multipole excitations summed over all states. In Fig. 14 we show the result of the calculation of the transverse form factors for the ^{7}Li nucleus.[59] There we also show the distribution functions for the contributions to the form factors corresponding to the spin-dipole and spin-octupole excitation operators. We see that at momentum transfers $q>1.5$ F^{-1} the spin-octupole type of excitation dominates not only in $M4$ and $E3$ transitions, but is also comparable to the second maximum of the spin-dipole matrix element of the $M2$-transition operator. The position of the extrema on the momentum-transfer axis depends weakly on the fact that the transverse form factors have been summed for each of the p-shell nuclei. The value of the total form factor (actually, $\Sigma_i F_i^2$) is more sensitive to the choice of nucleus. For example, for the ^{7}Li nucleus, as seen from Fig. 14, the sum $\Sigma_i F_i^2(M4)$ is larger than $\Sigma_i F_i^2(E3)$. On the contrary, for a nucleus at the end of the p shell, for example, ^{15}N, the sum of the squares of the $E3$ form factors is greater than $\Sigma_i F_i^2(M4)$. This is a consequence of the important role played by $p_{1/2} \to d_{5/2}$ transitions in the formation of the matrix elements of the operator $\hat{\mathcal{T}}_3^{\rm el}$ (see Fig. 15). The relative role of each excitation mode in forming the electron inelastic-scattering cross sections depends on the corresponding spectroscopic amplitudes, i.e., the structure of the wave functions of states with $J<J_0+4$.

The difference between the cross sections for electron elastic scattering for various multipole excitations becomes evident in the widths of the corresponding excited states. The decay widths are maximal for the excitations of lowest multipole order and minimal for $M4$ excitations. The decay widths for all J_0+4 states of p-shell nuclei are extremely small even for excitation energies $E>20$ MeV. For example, the total decay width of the state $|9/2^+, T=3/2;$

TABLE III. Lowest-energy states with spin J_0+4 of p-shell nuclei.

Nucleus	J^π, T	$E_{\rm theor}$, MeV	($E_{\rm exp}$, MeV)	$F_T^2 \cdot 10^4$ for $q=1{,}7$ F^{-1}	Dominant configuration in the wave function
^{7}Li	$11/2^+,1/2$	13,4		6,9	$(3^+, T=0; 2{,}14)\times(d_{5/2})_n$
^{10}B	$7^-,1$	22,0		0,23	$(9/2^-, 1/2; 11{,}0)\times d_{5/2}$
^{11}B	$11/2^+,1/2$	14,0	14,04	4,4	$(3^+, 0; 0)\times(d_{5/2})_n$
^{12}C	$4^-,1$	19,4	19,6	17,9	$(3/2^-, 1/2; 0)\times d_{5/2}$
^{13}C	$9/2^+,1/2$	9,46	9,50	2,3	$(2^+, 0; 4{,}44)\times(d_{5/2})_n$
^{14}C	$4^-,1$	11,48	11,72	7,3	$(3/2^-, 1/2; 3{,}68)\times(d_{5/2})_n$ $+(3/2^-, 1/2; 3{,}51)\times(d_{5/2})_p$
^{14}N	$5^-,1$	16,40	16,91	5,5	$(5/2^-, 1/2; 7{,}55)\times(d_{5/2})_n$ $+(5/2^-, 1/2; 7{,}38)\times(d_{5/2})_p$
^{15}N	$9/2^+,1/2$	11,01	10,68	1,76	$(2^+, 1; 7{,}01)\times(d_{5/2})_p$ $+(2^+, 1; 9{,}17)\times(d_{5/2})_n$

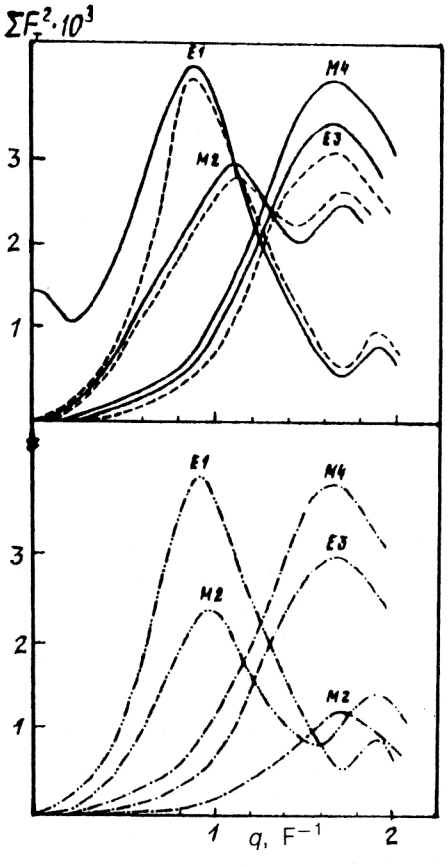

FIG. 14. Transverse form factors of $1\hbar\omega$ excitations of the ^{7}Li nucleus (Ref. 59). The solid lines are the total form factors, the dashed lines are the spin components of the total form factors, the dot–dashed lines are the contributions of the spin-octupole excitation operator, and the dashed lines with two dots are the contributions of the spin-dipole excitation.

$E=25$ MeV⟩ of the ^{15}N nucleus is only about 50 keV according to the calculation of Ref. 56, while for the state $|7/2^+, T=3/2;\ E=23.6$ MeV⟩ of the same nucleus the decay width is 1.4 MeV. The features of the structure of states leading to such large differences in the decay widths will be discussed in the next section for specific nuclei. However, the origin of this trend in the width distribution is rather general: states of lowest spin contain in their wave functions configurations constructed on lower-spin states of the final nuclei, and, in addition, may contain wave functions of a particle with angular momentum $l=0$, which is impossible for states of maximum spin with $J=J_0+4$. For nuclei with $J_0=0$, each excitation mode corresponds to a definite spin of the state, and the picture of the electroexcitation cross section for large scattering angles will be determined for $q>1.5$ F^{-1} by the contributions of $M2$, $E3$, and $M4$ transitions, with the latter forming narrow peaks in the cross section. For nuclei with $J_0\neq 0$ states with spins $J<J_0+4$ are populated by at least two multipole excitation channels. The identification of the spin in these cases is difficult, and study of the decay characteristics of multipole resonances can help.

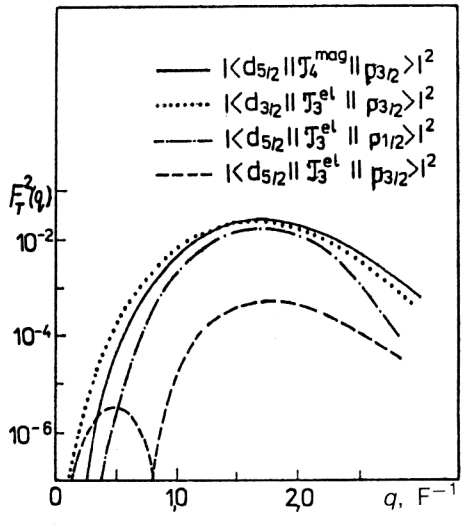

FIG. 15. Form factors of single-particle $M4$ and $E3$ excitations (Ref. 56).

3. PARTIAL CHARACTERISTICS OF $M4$ EXCITATIONS OF p-SHELL NUCLEI

The ^{7}Li nucleus

$M4$ excitations of the ^{7}Li nucleus lead to states with spins from $5/2^+$ to $11/2^+$ and isospins $T=1/2$ and $3/2$. The wave function of the state with maximum spin $11/2^+$, $T=1/2$ is formed (in the PNFS representation) by only a single configuration corresponding to a neutron in the $d_{5/2}$ state above the core—the ^{6}Li nucleus in the state $|3^+, T=0;\ E'=2.2$ MeV⟩. Since the decomposition of the wave function of the ground state of the ^{7}Li nucleus, according to Ref. 48, does not contain 3^+, $T=1$ configurations of the nucleus with $A=6$, the $11/2^+$ states with isospin $T=3/2$ are not excited in $M4$ transitions. This statement is based on the approximation in which only states with direct parentage relation to the ground state of the target nucleus are used as the states of the final core in the PNFS basis configurations (39). Extension of the PNFS basis by including hole states connected not to the ground state but to the lowest collective excited states of the target nucleus leads to the appearance of the $11/2^+$, $T=3/2$ state in the spectrum of $M4$ excitations of the ^{7}Li nucleus. Experimental study of the $M4$ excitations of the ^{7}Li nucleus and, in particular, understanding of the role of MSSs with $T=3/2$ might give some idea about the size of the contribution from interactions of doorway excitations with collective oscillations of the nucleus in MSS formation.

The lowest-energy state $9/2^+$, $T=1/2$, $E=14$ MeV also mainly corresponds to a "neutron–core" configuration. In decays of the $11/2^+$, $T=1/2$ and $9/2^+$, $T=1/2$ states localized at excitation energies of 14–15 MeV (see Fig. 12), the product nucleus ^{6}Li is formed primarily in the excited state with $E=2.2$ MeV. The decay widths are small and, according to the estimates of Ref. 59, amount to 0.02–0.05 MeV. The $7/2^+$ and $5/2^+$ nuclear states are also excited in $M4$ transitions, and these states are populated with greater probability than the $11/2^+$ and $9/2^+$ states.

The results of the theoretical calculation based on the PNFS version of the multiparticle shell model predict high

TABLE IV. Distribution of the squared form factor of $M4$ transitions in the ^{10}B nucleus.

J_f^π	7^-	6^-	5^-	4^-	3^-	2^-	1^-
$F_T^2(M4)\cdot 10^4$ for $q = 1{,}7$ F^{-1}	0,47	6,9	7,6	6,8	5,2	3,2	2,3

fragmentation of the $M4$-transition strength in the ^{7}Li nucleus, which is related both to the broad energy distribution of the excited states, and to the distribution of the transition strength among eight sets of states with different J and T.

The ^{10}B nucleus

The electroexcitation of $M4$ transitions in the ^{10}B nucleus occurs almost completely via the isovector channel and leads to the population of seven branches of $T=1$ states with spins from 1^- to 7^- (see Fig. 13). The calculation of the distribution of the $M4$-transition strengths in this nucleus reveals a significant fragmentation of these states in energy, which is a consequence of the complex parentage structure of the ^{10}B nucleus: removal of a $p_{3/2}$ nucleon from this nucleus leads to the appearance of a product nucleus in states distributed at energies above 12 MeV. The distribution of $M4$-transition strengths among different states of negative parity of the ^{10}B nucleus is shown in Table IV. The state of maximum spin, the 7^-, $T=1$ state, has the minimum probability for being populated in $M4$ transitions.

The ^{11}B nucleus

The complex structure of the excitation cross sections of the ^{11}B nucleus (like the ^{7}Li nucleus) at large momentum transfers (1–2 F^{-1}) is determined by the contributions to the cross sections of the large number of states belonging to the isospin branches $T=1/2$ and $T=3/2$. For $M4$ excitations these are states with spin $5/2^+$, $7/2^+$, $9/2^+$, and $11/2^+$, for $E3$ excitations they are states with spin from $3/2^+$ to $9/2^+$, and for $M2$ excitations they are states with spin from $1/2^+$ to $7/2^+$. For example, $5/2^+$ states are populated by all $1\hbar\omega$ excitation modes, the relative role of which changes as the momentum transferred to the nucleus grows. At excitation energies above 20 MeV, not only $M4$ transitions excited in the eight sets of levels, but also $E3$ and, to a lesser degree, $M2$ excitations must also contribute. This explains why the ^{11}B excitation spectrum[26] at large momentum transfers becomes a cross-linked broad peak. The separation of multipole orders from this broad peak requires careful analysis based on calculation of the q dependence of the individual spin states. For example, for $11/2^+$ states the q dependence must correspond to the graph of the $M4$ form factor. For states with spin $J<J_0+4$ it is the result of summing the contributions of the different multipole orders, the lowest of which give a large contribution at momentum transfers $q<1$ F^{-1}. The lowest-energy states of positive parity of the ^{11}B nucleus have been identified. In Table V we give the experimental data[65] for these states together with the results of the PNFS calculations.

In Fig. 11 we show the form factors of $M4$ excitations of the ^{11}B nucleus. An important feature of the picture of electroexcitation calculated for momentum transfers of about 1.7 F^{-1} is the strong $11/2^+$, $T=1/2$ level, the form factor of which exceeds that of the higher $9/2^+$ state by about a factor of two. As already shown in Table III, this level has a predominantly neutron configuration of a particle in the $d_{5/2}$ state and is excited in $(\pi^-,\pi^{-\prime})$ scattering. It decays exclusively to the 3^+, $T=0$ ground state of the ^{10}B nucleus, and the decay width is small (only about 97

TABLE V. Lowest-energy states of ^{11}B with spins $J^+\geqslant 5/2^+$.

J^+	T	E_{theor}	E_{exp}
11/2	1/2	14,0	14,04
9/2	1/2	11,7	11,26
7/2	1/2	7,0	9,18
7/2	1/2	12,8	10,6
7/2	1/2	14,6	12,02
7/2	1/2	18,2	13,6
7/2	3/2	15,18	15,3
5/2	1/2	7,28	7,29
5/2	1/2	8,54	9,27
5/2	3/2	14,25	14,34

keV), which corresponds to the experimental data.[26] The strength of $M4$ transitions to $11/2^+$ states with isospin $T=3/2$ is, according to the PNFS calculation, concentrated mainly in the two states with $E=21.28$ and 25.05 MeV. The first of these must decay via the proton channel with population of the 3^+, $T=1$, $E=9.02$ MeV level of the ^{10}Be nucleus. This level is unstable with respect to the neutron decay channel. A similar situation arises for the other states of positive parity of the ^{11}B nucleus located above 20 MeV. They undergo electrodisintegration either via the channel $(e,e'pn)$ or via the channel $(e,e'np)$, and the states with isospin $T=1/2$ decay primarily via the primary neutron channel. The two channels, proton and neutron, compete for states with $T=3/2$, but since the isobar-analog levels of the ^{10}Be nucleus lie considerably lower than the ^{10}B levels, the emission of primary protons in the decay of high-spin excitations of states with $T=3/2$ dominates. The angular distribution of the primary protons and neutrons from decay of the $11/2^+$ and $9/2^+$ states corresponds almost exclusively to nucleons with $l=2$.

The differences between the decay properties of states with isospin $T=1/2$ and $T=3/2$ are related to the structure of their wave functions and can be clearly traced in the PNFS approach. States of nuclei with $A-1$ can have isospin $T=0$ (states of only ^{10}B) and isospin $T=1$ (isobar-analog states in ^{10}B and ^{10}Be). If isospin is a good quantum number, core states with $T=0$ enter only into configurations with $T=1/2$. States with $T=3/2$ are constructed for both $T=0$ and $T=1$ configurations of the final nucleus with $A=10$. This leads to the predominantly neutron nature of the decay of the lowest-energy states with $J^\pi=11/2^+$ and $9/2^+$ with $T=1/2$ and the dominance of the primary proton channel in decays of states with $T=3/2$.

The PNFS calculation led to the conclusion that for the ^{11}B nucleus the high-spin states have a very large energy spread: the strength of the excited states becomes noticeable (above 10^{-5} in the form factor) in the energy range from 7 to 40 MeV. This situation is analogous to that in the dipole excitation of ^{11}B (Ref. 69) and is the consequence of the complicated parentage structure of the ground state of this nucleus and the isospin splitting.

The ^{12}C nucleus

In the field of high-spin magnetic excitations, the ^{12}C nucleus is a touchstone for experimental and theoretical studies, just as for other nuclear excitations. The $M4$ resonance in this nucleus, first discovered in the spectrum of electrons inelastically scattered on ^{12}C, has been well studied up to excitation energies of about 22 MeV, and combined studies in pion and electron beams now make it possible to determine the degree of isospin mixing typical for the 4^- states of this nucleus (Refs. 33, 66, and 34). The wave functions of the two orthogonal 4^- states at $E=19.25$ and 19.65 MeV, which were earlier thought to be states with $T=0$ and $T=1$, respectively, represent a mixture of $T=0$ and $T=1$ configurations:

$$|4^-,E=19.25\ \text{MeV}\rangle=\alpha|T=0\rangle-\beta|T=1\rangle;$$

$$|4^-,E=19.65\ \text{MeV}\rangle=\alpha|T=1\rangle+\beta|T=0\rangle.$$

Here the estimate of β, the amplitude of the admixture, rose from 0.32 (Ref. 66) to 0.6 ± 0.05 (Ref. 33) during the course of the investigations, which means that these two states mix strongly and should actually be viewed as proton and neutron states. Practically at the same time that the study of high-spin states began, strong suppression of the isovector $M4$ excitation mode was discovered in the ^{12}C nucleus: the ratio $S^2=F^2_{\text{exp}}/F^2_{\text{lim}}=0.37\pm0.04$ for the level at 19.65 MeV, to which a purely isovector amplitude had previously been assigned. The inclusion of the isospin mixing does not change anything, but even slightly exacerbates the problem: according to the data of Ref. 33, the total square of the isovector amplitudes in the two states at 19.65 and 19.25 MeV is only about 0.3. In the calculation based on the PNFS approach, the influence of two factors on the value of the spectroscopic amplitude has been analyzed: the deviation of the nuclear ground state from the closed $p_{3/2}$ shell and the spread of the $M4$-transition strength among several 4^- states within the isospin representation. Use of the functions[47,48] for the ground state of the ^{12}C nucleus leads to at least two 4^- states with given isospin $T=0$ or $T=1$, since with probability 0.71 the removal of a nucleon in the $p_{3/2}$ state leads to the formation of a product nucleus in the ground state $(3/2)_1$, and with a probability of about 0.1 it leads to the removal of one in the excited state $(3/2)_2$. About 20% of the separation probability can be attributed to the $p_{1/2}$ nucleon, i.e., it does not lead to $M4$ excitations.

The calculation of the 4^-, $T=1$ states for this restricted basis gives two levels at energies of about 19 and 25 MeV with the distribution of the $M4$-transition strength between them close to 7:1. The interaction of doorway excitations with quadrupole oscillations of the nuclear surface plays an important role for the ^{12}C nucleus. In Ref. 58 the 4^- states were calculated for an extended basis including those configurations of the final nucleus with direct parentage connection to the ^{12}C ground state and configurations related to the 2^+, $T=0$, $E=4.44$ MeV state. This procedure extended the basis from 2(4) to 8(16) configurations (the numbers in parentheses correspond to the use of the proton–neutron rather than the isospin representation). This extension of the basis does not lead to any significant change in the spectroscopic amplitudes of the lowest 4^- states from the results obtained with the smaller basis. The distribution that is obtained is shown in Fig. 11. According to this calculation, the lowest state, the 4^-, $T=1$ state, should decay primarily via the proton channel to the ground state of ^{11}B. The ratio of the probabilities for populating the ground states of ^{11}C and ^{11}B is about 6:94. The total width of the state is about 90 keV, which is consistent with the available data.[34,33] The 4^-, $T=1$ state at $E=25.10$ MeV of second-highest intensity of the $M4$ excitation has a form factor roughly an order of magnitude smaller than that of the principal 4^-, $T=1$ peak. The largest probability is for this state to decay to the first $(5/2)^-_1$ state of the ^{11}B nucleus, to excited $(3/2)^-_2$ states of

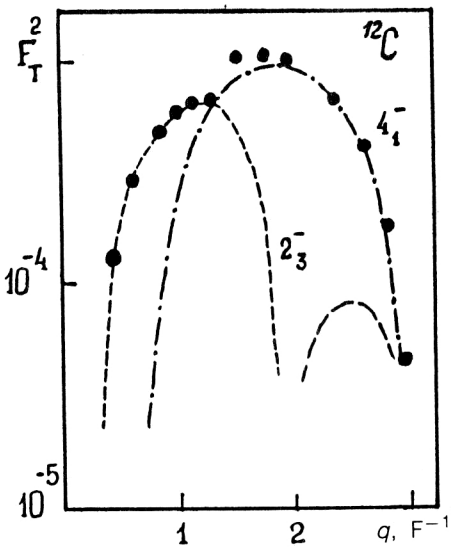

FIG. 16. Transverse form factor of the complex at 19.5 MeV in the ^{12}C nucleus. The points are from the experiments of Refs. 2 and 34. The dashed line is the $M2$ form factor, and the dot–dashed line is the $M4$ form factor. The results of the calculations using the PNFS approach are multiplied by 0.7.

the ^{11}B and ^{11}C nuclei, and to the $(7/2)_1^-$ state of the ^{11}B nucleus.

The ratio of the transverse form factors of isovector $M2$ and $M4$ excitations in the energy range 18–20 MeV obtained in the PNFS calculation corresponds to the experimentally observed ratio[2,34] (Fig. 16). The measured form factor $F_T^2(q)$ is the sum of the form factors of the 2^-, $T=1$, $E=19.2$ MeV and 4^-, $T=1$, $E=19.4$ MeV levels (here we give the theoretical values of the energy). The problem of the suppression of isovector $M4$ excitations of light nuclei can be solved by improving the microscopic description of the wave functions of the ground and excited nuclear states. The use of the functions of the PNFS approach gives for the square of the spectroscopic isovector amplitude of the lowest-energy 4^- state the value 0.68–0.71 instead of 1, the result of the limiting model, in which the ^{12}C nucleus is viewed as the closed subshell $(p_{3/2})^8$. These values were obtained in calculations using the HOWFs. However, since as a rule the MSSs lie at excitation energies above the nucleon separation threshold, the radial function of the particle in the final potential, for example, in the Woods–Saxon potential (the WSWF), can differ significantly from the oscillator function, and the overlap integral $\langle j_2 | j_{J-1}(qr) | j_1 \rangle$ will be different for protons and neutrons. The effect of the WSWFs on the overlap integral, the form factor, and the spectroscopic amplitudes has been estimated in Ref. 67 for various nuclei with closed subshells. The use of the WSWFs has the greatest effect for light nuclei, where the result of the WSWF calculation differs from that of the HOWF calculation by a factor of 2.4 in the case of ^{12}C and a factor of 1.5 in the case of ^{16}O. For intermediate nuclei the results of the two calculations nearly coincide, and for the heavy ^{208}Pb nucleus the square of the spectroscopic amplitude in the WSWF approach is even larger than in the HOWF approach. (The tendency for the effect of the final potential to be diminished reflects the increasing importance of the centrifugal potential in forming the radial function of the unbound nucleon.) In Table VI we compare the isovector spectroscopic amplitudes of the lowest-energy 4^- state of the ^{12}C nucleus in different versions of the calculation.

TABLE VI. Ratio of the squared form factors F_T^2/F_{lim}^2 for the 4^-, $E=19.6$ MeV state of the ^{12}C nucleus.

Experiment	Limiting model, HOWFs	PNFS, HOWFs	Limiting model, WSWFs	PNFS, WSWFs
0.37–0.3	1	0.68–0.71	0.42	0.30–0.29

Thus, the use of realistic representations of the microscopic structure of the wave functions of nuclear states and nucleons leads to a result which agrees nearly completely with experiment. We recall that the theoretical result should be increased by 12–18% if, in addition to the purely spin term, meson exchange currents are also included in the calculation of the form factor.

The ^{13}C nucleus

The structure of the basis configurations of excited $9/2^+$ states of the ^{13}C nucleus is very simple: all the configurations are constructed on 2^+ states of nuclei with $A=12$. The $9/2^+$, $T=1/2$ wave functions involve both $(2^+,T'=0,E')\times(d_{5/2})_n$ configurations, where E' are the excitation energies of the three 2^+, $T=0$ states of the ^{12}C nucleus, and $(2^+,T'=1,E')\times(d_{5/2})_{n,p}$ configurations, where the 2^+, $T'=1$ states enter into the spectrum of the nuclei ^{12}B and ^{12}C. Of the six $9/2^+$, $T=1/2$ states, only two have significant $M4$-transition strengths. This is consistent with the experimental data.[35] The neutron nature of the lowest-energy state, the $9/2^+$, $T=1/2$ state, was discussed above. Here the theoretical PNFS calculation leads to a spectroscopic-amplitude distribution close to the experimental one (Table VII).

The structure of the $M4$ excitations of the ^{13}C nucleus at excitation energies above 19 MeV is determined by the

TABLE VII. Spectroscopic amplitudes of the lowest state with $J^\pi=9/2^+$, $T=1/2$ of the ^{13}C nucleus.

Data	$\mathcal{Z}_0$	$\mathcal{Z}_1$
PNFS calculation	−0,31	−0,23
Experiment (Ref. 35)	0,26 ± 0,07	+0,28 ± 0,02

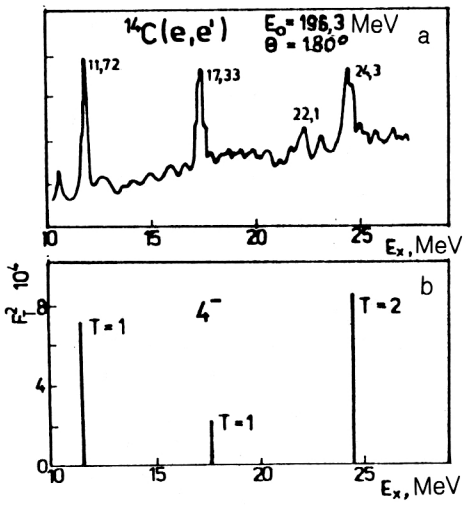

FIG. 17. Excitation-energy distributions of the cross section for $^{14}C(e,e')$ from the experiment of Ref. 36 (a) and calculated in Ref. 55 for $q=1.8$ F^{-1} (b).

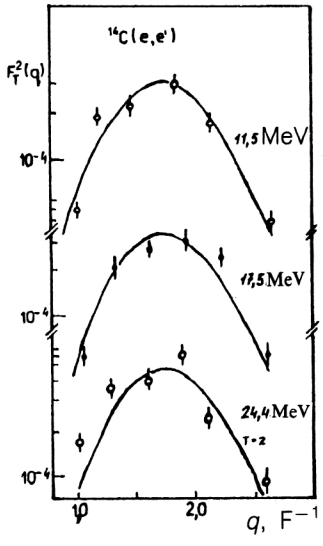

FIG. 18. Form factors of 4^- states of the ^{14}C nucleus. The points are from Ref. 36, and the curves are the result of the calculation of Ref. 55 (see Table VIII).

contributions of states with both $T=3/2$ and $T=1/2$, but the principal maximum of the excitation corresponds to the $9/2^+$, $T=3/2$ level. The experimental value of the energy of the principal peak is 21.47 MeV, while the PNFS calculation gave 22.8 MeV. (It should be noted that the calculations for states with $T=1/2$ and $T=3/2$ were carried out using the same set of Hamiltonian parameters.) The structure of the isovector $M4$ excitations shown in Fig. 11 corresponds to the experimental result in Fig. 8. Calculation of the decay widths and population probabilities of levels of the final nuclei showed that the proton decay width of the $9/2^+$, $T=3/2$, $E=22.8$ MeV state is 2.5 times larger than the neutron width, and the total decay width is 0.3 MeV. There is a 72% probability for decay to the level $|2^+, T'=1, E'=0.95$ MeV$\rangle$ of the ^{12}B nucleus, and a 28% probability for decay to the level $|2^+, T'=1, E'=16.11$ MeV$\rangle$ of the ^{12}C nucleus. Both of these states are unstable with respect to emission of a gamma ray.

The ^{14}C nucleus

The calculation of $M4$ excitations of the ^{14}C nucleus includes among the states of the final nuclei the three lowest $3/2^-$, $T=1/2$ states of the ^{13}C nucleus (3.68, 9.9, and 11.8 MeV) and the $3/2^-$, $T=3/2$ states ($E=15.11$ MeV in ^{13}C and $E=0$ in ^{13}B). In Fig. 17 we show the results of the calculation for the 4^- states and the experimental data[36,23] for the same momentum transfer to the nucleus. The behavior of the form factors $F_T^2(q)$ of the three strong states is shown in Fig. 18. The qualitative agreement between the PNFS calculation[55] and experiment[36,23] is completely satisfactory regarding both the location of the peaks and their relative intensity. The curves in Fig. 18 have been renormalized by the factors S^2, which are considerably closer to unity in the PNFS calculation with HOWFs than in the limiting model. These quantities are given in Table VIII.

The use of realistic functions in the case of ^{14}C therefore again leads to an $M4$-transition strength distribution closer to experiment. The total transverse form factor $\Sigma F_T^2(q)$ exceeds the value obtained in the experiment of Ref. 23 by a factor of about 1.7–1.9. As already shown above for the ^{12}C nucleus, the use of the WSWFs instead of the HOWFs decreases the overlap integral of the radial wave functions. This effect is more pronounced for the 4^-, $T=2$ state, and the decrease of the form factor calculated in the PNFS approach with the HOWFs ensures in this case not only qualitative but also quantitative agreement with experiment for the most intense 4^-, $T=2$ $M4$-excitation peak.

The radial characteristics of the $M4$ resonances of the ^{14}C nucleus are given in Table IX (the PNFS calculation with HOWFs).

In the absence of isospin mixing of states, the principal peak of the $M4$ excitations with the quantum numbers 4^-, $T=2$ should decay via the proton (82% probability) and neutron channels to the lowest states of the ^{13}C and ^{13}B nuclei with isospin $T=3/2$. The isospin mixing of resonance states with $T=2$ and $T=1$ opens up channels for the decay of the principal maximum of the $M4$ excitation to the lowest states with $T=1/2$ of the ^{13}C nucleus with spin $J=3/2^-$. This effect should be clearly seen in the neutron decay spectra, since the decay to the $3/2^-$, $T=1/2$, $E=3.68$ MeV state will be accompanied by the emission of hard neutrons with $\varepsilon_n \cong 12$ MeV. The ratio of the widths of the isospin-allowed and forbidden neutron channels is very sensitive to the isospin-mixing parameters, as shown by the calculation of Ref. 55. The width of the decay of the 4^-, $T=2$ resonance to the $3/2^-$, $T=1/2$, $E=3.68$ MeV state via the neutron channel is increased by a factor of 40 as the Coulomb mixing parameter varies from 0.1 to 0.5 MeV. Measurement of the hard neutrons from the decay of excited 4^- states in conicidence with the

TABLE VIII. Energies and factors $S^2=(F_T^2)_{exp}/(F_T^2)_{theor}$ for 4^- states of the ^{14}C nucleus.

E_{exp}, MeV	E_{theor}, MeV	S^2, limiting model (HOWFs), Ref. 36	S^2, PNFS (HOWFs), Ref. 55
11,72	11,5	0,19	0,40
17,33	17,5	0,22	1,20
24,3	24,4	0,37	0,57

γ rays from deexcitation of the 3.68 MeV level can serve as a measure of the isospin mixing.

The ^{14}N nucleus

The energies and wave functions of all the excited states of negative parity corresponding to $1\hbar\omega$ excitations[68] of the ^{14}N nucleus have been obtained in the PNFS approach with a single set of Hamiltonian parameters. States with spin 3^-, 4^-, and 5^- are excited in $M4$ transitions. In Figs. 19 and 20 we compare the results of the PNFS calculations for the isovector transverse form factors of ^{14}N with the data of the (e,e') experiment[37] (see also Figs. 8 and 11). The calculation[68,55] reproduces the general structure of the $M4$ transitions, but gives a richer distribution spectrum for them. We note that the experimental isolation of $M4$ peaks is difficult for the complicated structure of the $^{14}N(e,e')$ cross section, and some low-intensity peaks remain unidentified. This is one of the sources of suppression of the MGR strengths.

The principal peak of the $M4$ excitation with spin 5^- and $T=1$ was found at $E=16.9$ MeV. The theory reproduces the position (16.4 MeV) and form factor of this resonance. The second peak with $J^\pi=5^-$, $T=1$ is also reproduced, although its location is theoretically overestimated. The calculation predicts two resonance peaks near the main one with the quantum numbers 3^- and 4^-, $T=1$. The first is about four to five times lower, and the second is three times lower in intensity than the 5^- peak at $E=16.4$ MeV. The data[37] also suggest the presence of two peaks in this region with energies of 16.7 and 17.2 MeV, with their quantum numbers not yet determined. The calculation gives three resonance $M4$-excitation states in the energy range 11–16 MeV. The experimental data indicate the presence of several peaks, among which the one located at 15 MeV displays the typical behavior of an $M4$ form factor. Theory (see Fig. 20) shows that this peak should be identified as a 3^-, $T=1$ state. At excitation energies $E>18$ MeV a peak is clearly seen experimentally at $E=20.1$ MeV, and the other peaks in this region (at $E=17.8$, 18.5, and 19.7 MeV) have lower intensity. According to the theoretical estimates, the most likely candidate for the peak at 20.1 MeV is the $M4$ resonance with the quantum numbers 4^-, $T=1$. The identification of the spin of the excited state, i.e., in this case the choice between 3^-, 4^-, and 5^- isovector excitations, using the value of the $M4$-transition form factor, is ambiguous, since the curves for the $M4$ form factors are similar. Moreover, the location of the MGR in the theoretical calculation depends on the choice of Hamiltonian parameters, and in the calculation using a single parameter set for all multipole orders it cannot be determined to better than ± 1 MeV. In this situation a promising method for identifying the spin of the state might be to study the partial decay channels of the excited states (Table X).[68]

For the 5^-, $T=1$ state at 16.4 MeV the only open decay channel is that of proton decay with formation of the final nucleus ^{13}C in the excited state $5/2^-$, $E=7.55$ MeV and emission of a d proton with energy 1.75 MeV. The first $5/2^-$ state of the ^{13}C nucleus is unstable with respect to neutron decay to the ground state of ^{12}C. Decays to excited states of ^{12}C are energetically impossible. This makes it possible to predict the energy location of the neutron peak of the second decay: $\varepsilon_n=E-E_b=2.6$ MeV. This peak in the neutron spectrum should be split, reflecting the angular anisotropy of the d protons of the first stage of the decay of the resonance state. In the theoretical PNFS calculation the channels for decay of the 5^-, $T=1$ states to the ground

TABLE IX. Form factors and decay characteristics of 4^- states of the ^{14}C nucleus.

Energy E, MeV	Isospin T	$F_T^2\cdot 10^4$	Widths and population probabilities of levels of nuclei with $A=13$							
			$^{14}C \to {}^{13}C + n$					$^{14}C \to {}^{13}B + p$		
			J'	$3/2^-$	$3/2^-$	$3/2^-$	$3/2^-$	Γ_n, MeV	J'	$3/2^-$	Γ_p, MeV
			T'	1/2	1/2	1/2	3/2		T'	3/2	
			E'	3,68	9,9	11,9	15,1		E'	0	
11,5	1	7,3						0			0
17,5	1	2,2		100				0,1			0
19,4	1	10^{-3}		45	55			0,1			0
23,4	1	$\sim 10^{-4}$		17	2	71		0,5		10	0,06
24,4	2	8,7					18	0,07		82	0,3

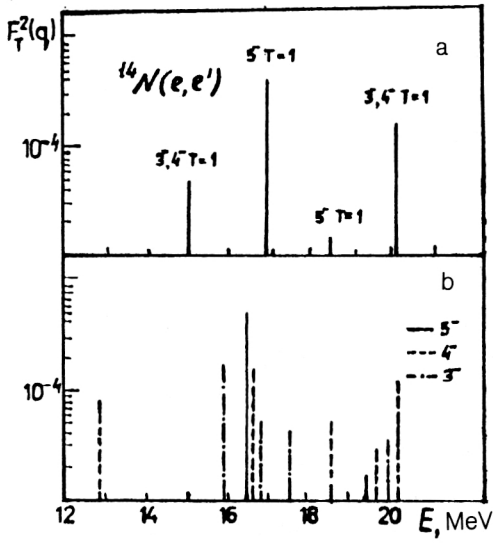

FIG. 19. Excitation-energy distribution of $M4$ form factors of the ^{14}N nucleus from the experiment of Ref. 37 (a) and calculated in Ref. 55 (b).

state and the lowest $3/2^-$ excited states of the ^{13}C and ^{13}N nuclei are closed.

There are several features distinguishing decays of the 3^- and 4^-, $T=1$ states located near the principal 5^-, $T=1$ peak from the decay of this peak. The two states predominantly decay to the lowest $3/2^-$, $T=1/2$ states of ^{13}C and ^{13}N. For the 3^-, $T=1$ state decay to the ground states of these nuclei is possible, and must be manifested as peaks at high energies in the spectra of electrodisintegration nucleons ($\varepsilon_p \cong 9$ MeV, $\varepsilon_n \cong 6$ MeV). The emission of high-energy protons and neutrons is also characteristic of

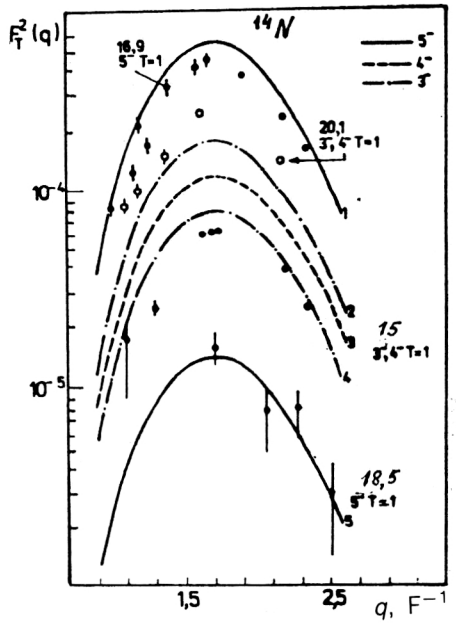

FIG. 20. Form factors of $M4$ excitations of the ^{14}N nucleus. The points are from Ref. 37, and the curves are from Ref. 55. The numbers from 1 to 5 on the curves correspond to the states with energies 16.4, 16.0, 20.2, 16.9, and 19.5 MeV (see Table X) (Ref. 55).

the decay of the 3^-, $T=1$ maxima located near 20 MeV, since for these states the channel of decay to the ground state of nuclei with $A=13$ is open, while it is closed for the 4^- and 5^- states. Decays of the 4^- and 5^- states, and also secondary decays of excited states of nuclei with $A=13$ populated with sizeble intensity in the decay of $M4$ resonances of the ^{14}N nucleus, lead to the emission of softer nucleons ($\varepsilon_p \lesssim 3$ MeV). The difference between the decay characteristics of the 3^- and 4^- states is strongly manifested at excitation energies $E \approx 16$ MeV, since here the resonance widths are small, and the 3^- states decay predominantly to the ground states of the daughter nuclei, i.e., via a channel closed for decays of the 4^- and 5^- states.

The study of the decay characteristics of $M4$ resonances in the case of ^{14}N is therefore a promising method for identifying the quantum numbers of excited nuclear states.

The ^{15}N nucleus

High-spin excitations of the ^{15}N nucleus were analyzed in Ref. 38, where both data from $(\pi^+,\pi^{+\prime})$ and $(\pi^-,\pi^{-\prime})$ experiments on this nucleus and data from (e,e') experiments were used. The latter had previously been described only in a preliminary publication.[72] The region of detailed investigations using pion beams was restricted to the excitation energy 18 MeV. The identification of the peaks in the differential (π,π') cross sections as excitations of the magnetic type with $\Delta S=1$ was done using the dependence of the cross section on the pion kinetic energy for fixed (1.57 F^{-1}) momentum transfer. The peaks of the cross section at excitation energies of 10.69, 12.49, and 17.2 MeV fell sharply with increasing T_π. The state with $E=14.0$ MeV displayed a less abrupt falloff with the pion energy. Attempts were also made to extract the $M4$ peaks from the region of excitation energies above 18 MeV, where according to the data of Ref. 72 several strong maxima of the (e,e') cross sections should be concentrated. Analysis of the data of (π,π') experiments gave two solutions for the spectroscopic amplitudes $\mathscr{Z}_0$ and $\mathscr{Z}_1$ of all the intense peaks of the cross section, which were treated as $M4$-transition peaks.

Theoretical study of all the $1\hbar\omega$ transitions in the ^{15}N nucleus showed[56] that at momentum transfers above 1.5 F^{-1}, where the $M4$-transition form factors are located near the maximum, transitions with lower multipole order are still fairly important. A particularly important contribution to the excitation cross section comes from the $E3$ excitation, the principal maximum of which is formed by the $p_{3/2} \to d_{3/2}$ and $p_{1/2} \to d_{5/2}$ transitions (see Fig. 15). The large contribution of the latter to the transverse form factor $F_T(E3)$ makes it necessary to carry out a combined analysis of the $M4$ and $E3$ excitations for nuclei at the end of the p shell. The distribution of the transverse form factors of $M4$ and $E3$ excitations populating the $9/2^+$, $7/2^+$, and $5/2^+$ states of the ^{15}N nucleus is shown in Fig. 21. The calculation was performed using the PNFS version of the shell model, and within a unified approach it was possible to obtain all the wave functions for the $1\hbar\omega$ excitations of this nucleus. The dependence of the excitation cross sec-

TABLE X. Level population probabilities (in %) of ^{13}C and ^{13}N nuclei in the decay of high-spin J^-, $T=1$ states of the ^{14}N nucleus and decay widths Γ.

State J^π	E, MeV	$^{14}N \to {}^{13}C + p$							$^{14}N \to {}^{13}N + n$							Γ_p, keV	Γ_n, keV	Γ_{tot}, keV
		$J^-=1/2$	1/2	1/2	3/2	3/2	5/2	5/2	1/2	1/2	1/2	3/2	3/2	5/2	5/2			
		$E'=0,0$ MeV	8,86	11,08	3,68	9,90	7,55	10,82	0,0	8,92	10,83	3,51	9,48	7,39	10,36			
5^-	16,37						100,0									6		6
	19,45						24,9	67,9						7,2		4	0	4
4^-	12,94				100,0											20		20
	16,62				49,1		24,9					26,0				34	12	46
	18,66				10,7	6,0	69,0					8,4		5,8		14	2	16
	19,73				0,6	2,0	71,1	0,1				0,5		25,7		377	134	501
	20,21				0,0	20,9	52,7	1,7				0,0	0,0	24,7		241	80	321
	23,82				0,0	1,7	1,0	56,6				0,0	1,4	0,9	38,4	765	523	1288
3^-	8,21	100														1		1
	12,68	60,5			15,1				24,5							50	16	66
	15,99	20,3			44,3		1,3		16,6			17,6				56	29	85
	16,93	8,0	0,0		53,6		0,2		6,9			31,4				503	312	815
	17,66	4,3	0,1		53,1	0,0	2,0		3,9			36,7				450	300	750
	19,09	1,5	8,0	0,0	3,6	1,0	56,9	0,0	1,4			3,0		24,5		222	90	312
	19,98	19,3	0,1	0,5	1,2	10,5	31,9	3,6	18,3	0,0		1,1		13,5		160	79	239
	20,35	0,8	6,4	2,8	20,9	15,8	13,5	8,7	0,8	0,7		18,7	0,2	10,7		140	63	203
	21,02	0,6	1,0	0,1	0,9	1,2	53,7	0,0	0,7	0,3		0,8	0,2	40,6		1160	855	2015

tions on the choice of parameters of the residual-interaction Hamiltonian was also studied. The analysis of Ref. 56 revealed a relatively weak dependence of the distribution of the excitation cross sections on the choice of residual-interaction parameters, even for the giant-dipole-resonance cross sections, where configuration mixing and collectivization of states play the most important role.

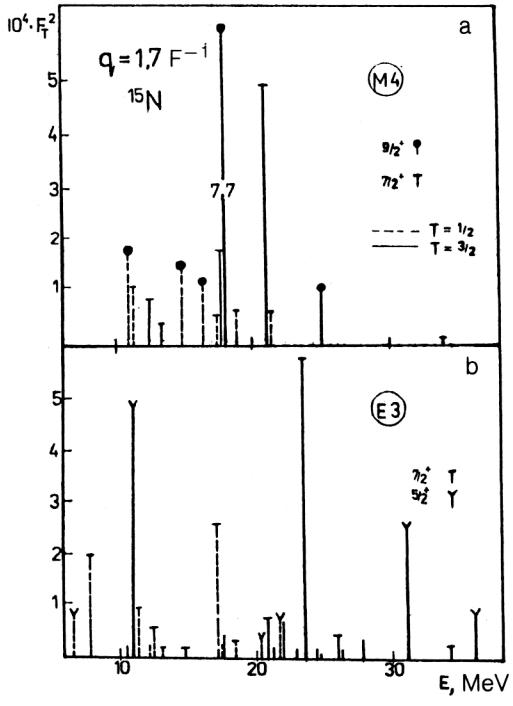

FIG. 21. Energy distribution of the form factors of $M4$ and $E3$ excitations of the ^{15}N nucleus for $q=1.7\ F^{-1}$ (Ref. 56).

The effect of the choice of parameters for the residual-force calculation is even less important for excitations of high-spin states than for $E1$ excitations. A more important factor for high-spin excitations was the choice of the set of basis configurations: restricting them to only those states of the final nucleus which have a direct parentage relation to the ground state of ^{15}N, or extension of the basis to include the configurations corresponding to the interaction of doorway excitations with phonons. Comparison of the results of the calculation for the "small" and "large" bases showed that the second version of the calculation more realistically reproduces the experimental picture of high-spin excitations. The values of the spectroscopic amplitudes are especially sensitive to the details of the theoretical model. To illustrate this, let us compare the experimental and theoretical results for the spectroscopic amplitudes $\mathscr{Z}_{4,T}$ of the first two excited states in the excitation spectrum of ^{15}N. The two solutions from analysis of (π,π') experiments give ratios $\mathscr{Z}_0/\mathscr{Z}_1$ with the same sign for the excitation energies 10.7 and 12.5 MeV; here for the first solution $\mathscr{Z}_0/\mathscr{Z}_1=-0.95$, and for the second $\mathscr{Z}_0/\mathscr{Z}_1=-0.27$ for the first of the excited states. The solution for $\mathscr{Z}_0/\mathscr{Z}_1$ in the PNFS approach[70] depends on the choice of basis: in the small basis $\mathscr{Z}_0/\mathscr{Z}_1=14.1$, and in the large one it is 1.4 for the first state, the $9/2^+$, $T=1/2$ state (see Table XI).

The level at 14.04 MeV, according to the experiment of Ref. 38, is excited by both $\Delta S=1$ and $\Delta S=0$ transitions. It is natural to identify it with the $7/2^+$, $T=1/2$ state, the excitation of which contains contributions from both $M4$ transitions with $\Delta S=1$ and $E3$ transitions for which there can be contributions from $\Delta S=1$ and $\Delta S=0$ excitations.

The position of levels with isospin $T=3/2$ is somewhat too low in excitation energy compared with the data.[38] The calculation of Ref. 56 indicates three principal $T=3/2$

TABLE XI. Characteristics of levels with $I=7/2,9/2$ (large basis): energies, spectroscopic amplitudes, maximum values for the transverse form factors, and level widths for the ^{15}N nucleus.

$2I$	$2T$	E, MeV	$\mathscr{Z}'_0$	$\mathscr{Z}_1$	$10^4\cdot F^2_{M4}$	$10^4\cdot F^2_{E3}$	$10^4\cdot F^2_T$	$10^4\cdot F^2_{C3}$	Γ, keV
9	1	11,00	−0,314	−0,214	1,76	0	1,76	0	0
9	1	11,73	0,665	−0,080	0,05	0	0,05	0	0
9	1	14,9	0,046	−0,250	1,37	0	1,37	0	0
9	1	16,40	0,047	−0,233	1,19	0	1,19	0	0
9	1	21,38	−0,071	−0,122	0,43	0	0,43	0	96
9	3	17,95	0	−0,572	7,70	0	7,70	0	0,5
9	3	25,02	0	−0,207	1,01	0	1,01	0	46
7	1	7,84	0,129	−0,032	0,001	1,91	1,91	2,16	0
7	1	11,35	−0,187	0,259	1,18	0,02	1,20	0,06	0
7	1	11,44	0,221	−0,071	0,02	0,84	0,86	7,14	0,4
7	1	12,59	0,137	0,157	0,78	0,53	1,32	3,28	25
7	1	13,32	−0,155	0,125	0,22	0,22	0,44	1,72	1
7	1	17,51	−0,175	−0,100	0,41	2,53	2,91	5,67	265
7	1	17,58	0,059	0,043	0,07	0,35	0,42	0,73	1915
7	1	18,79	0,353	0,091	0,58	0,30	0,88	0,78	10
7	1	19,96	−0,038	−0,011	0,01	0,06	0,07	4,70	555
7	1	21,11	−0,294	−0,090	0,50	0,02	0,51	0,001	196
7	1	23,53	−0,202	0,044	0,00	0,001	0,002	0,13	299
7	1	27,99	0,032	−0,020	0,01	0,18	0,18	0,52	101
7	3	17,69	0	−0,272	1,75	0,39	2,14	2,78	0
7	3	21,22	0	−0,452	4,81	0,73	5,54	0,13	28
7	3	23,57	0	−0,086	0,17	5,78	5,95	10,53	1403
7	3	26,10	0	−0,069	0,11	0,45	0,57	0,17	120
7	3	34,13	0	−0,076	0,14	0,23	0,37	0,04	2643

peaks at excitation energies above 17 MeV; the lowest of these peaks corresponds to the $9/2^+$, $T=3/2$ state and is excited only in $M4$ transitions.

The spectroscopic amplitudes $\mathscr{Z}_0$ and $\mathscr{Z}_1$ obtained in Ref. 38 for $M4$ transitions in the ^{15}N nucleus are $\mathscr{Z}_0=+0.238\pm0.015$ and $\mathscr{Z}_1=-0.252\pm0.030$ for the 10.7 MeV state and $\mathscr{Z}_0=+0.294\pm0.018$ and $\mathscr{Z}_1=-0.334\pm0.036$ for the 12.5 MeV state. [The definition (19) of the spectroscopic amplitudes was used in Ref. 38.] If both these states are identified with $9/2^+$, $T=1/2$ levels, the theoretical interpration of the ratios of the signs of these amplitudes is difficult. If the wave functions of the first two $9/2^+$ levels are orthogonal, the spectroscopic amplitudes should have, roughly speaking, different ratios of the signs. We note that these calculations, carried out in Ref. 38 for single-particle matrix elements of the $9/2^+_1$ and $9/2^+_2$ states, obtained in a version of the shell model similar to the PNSF version but with different interaction parameters,[22] also give different ratios of the signs of the $\Delta T=0$ and $\Delta T=1$ matrix elements for these states. It is possible that the discrepancy between experiment and theory here is related to the curious contradiction between the predictions of the calculations of Refs. 47 and 48 for states with parity equal to that of the ground state, and the data from (p,d) reactions. According to Ref. 48, in the spectrum of nuclei with $A=14$ there should be only one state with $(J^\pi,T)=(2^+,1)$ which has a significant parentage connection to the ground state of the ^{15}N nucleus and must therefore be manifested in capture reactions. The experiment of Ref. 71 indicates the excitation of two close 2^+, $T=1$ states with energies 9.17 and 10.43 MeV with similar spectroscopic factors of the (p,d) reaction. It is possible that the similarity of the microscopic structures of the first $9/2^+$, $T=1/2$ states, which is manifested in their spectroscopic amplitudes $\mathscr{Z}_0$ and $\mathscr{Z}_1$, is a consequence of the "doublet" structure of the hole states of the final nuclei with $A=14$.

The decay characteristics of high-spin states of the ^{15}N nucleus are given in Table XII from the results of the calculation of Ref. 70. Decays of $9/2^+$ states are blocked up to excitation energies of 17 MeV, since, according to the calculations of Ref. 70, nucleon decays of $9/2^+$ states lead to states of the final nuclei ^{14}N and ^{14}C with energies of 7 MeV and higher. Decays of $9/2^+$ states lying above 17 MeV are very sensitive to the features of the configuration structure of the excited-state wave functions. The extension of the basis to 3^+, $T=0$ states of the final nuclei opens up channels with large relative probability in the decay of high-lying $9/2^+$ levels. The isospin branch $9/2^+$, $T=1/2$ decays primarily via the neutron channel to $T=0$ states of ^{14}N. The $T=3/2$ isospin branch is characterized by change in the ratio of the proton and neutron channels as the excitation energy increases. Proton channels dominate in decays of $9/2^+$ and $7/2^+$ states with $T=3/2$ and $E<24$ MeV, and neutron channels dominate for $E>24$ MeV. This result of the model calculation is, however, based on the use of the isospin representation. Study of the partial decay channels of states with maximum spin together with determination of the spectroscopic amplitudes is the most promising way of investigating the microscopic structure of excited states and checking the validity of model approximations.

CONCLUSION

The study of excited states of nuclei arising from $MJ_{\max}$ transitions is the most direct route to understanding

TABLE XII. Decay characteristics of states with $I=7/2,9/2$ from the calculation using the large basis for the ^{15}N nucleus.

I,T	E, MeV	Widths, keV			Level population probabilities of nuclei $A=14$, %									
					^{14}C		^{14}N							
		Γ_{tot}	Γ_p	Γ_n	2,1 7,0	2,1 17,9	1,0 0,0	1,0 3,95	3,0 6,45	2,0 7,03	3,0 9,13	2,1 9,17	1,0 15,2	2,1 17,9
	11,0	0	0	0										
9/2,	11,7	0	0	0										
1/2	14,9	0	0	0										
	16,4	0	0	0										
	21,4	96	0	96					23,3	52,0	24,7	0,1		
9/2,	18,0	0,5	0,5	0	100									
3/2	25,0	46	18	28	39,7							60,3		
	7,8	0	0	0										
	11,40	0	0	0										
	11,44	0,4	0	0,4			100							
	12,6	25	0	25			100							
	13,3	1	0	1			100							
7/2,	17,5	265		265			3,7		94,3					
1/2	17,6	1915	0	1915					100					
	18,8	10	3,5	6,5	34,9		7,3	31,3	25,5	1,0				
	20,0	555	29	526	5,2		31,4	0,5	0,9	62,0				
	21,1	196	0,6	195	0,2		0,7	12,4	13,7	23,4	49,5			
	23,5	299	3	296	0,3		0,1	1,6	8,0	5,4	83,7			
	28,0	101	17	84	14,8		2,2	5,9	10,1	5,6	16,3	6,6	36,3	
	17,7	0	0	0										
7/2,	21,2	28	20	8	72,1							27,9		
3/2	23,6	1403	626	777	44,5							55,4		
	26,1	120	46	74	37,0							60,8		
	34,1	2463	709	1934	1,5	22,8						2,9		65,6

the structure and properties of the spin component of the nuclear nucleon current. The combined analysis of (e,e'), $(\pi^-,\pi^{-\prime})$, and $(\pi^+,\pi^{+\prime})$ reactions exciting MJ_{max} transitions for momentum transfer to the nucleus in the range 1.5–2 F^{-1} makes it possible to obtain the spectroscopic amplitudes of excited states, which is today the most detailed information available about the nuclear wave functions. This unique possibility offered by MJ_{max} excitations makes them an important tool for checking microscopic methods of describing nuclear states.

For p-shell nuclei, whose ground state does not correspond to a filled shell, the most important factor in the formation of the energy distribution of the cross sections of $M4$ transitions in the target nucleus A is the spread of the hole states over the excitation energies of the final nuclei $A-1$. This conclusion of the theoretical analysis based on the PNFS version of the multiparticle shell model is confirmed by comparing the calculated $M4$ form factors with the experimental data. The PNFS version of the multiparticle model also allows the interpretation of the ratio of the $(\pi^-,\pi^{-\prime})$, and $(\pi^+,\pi^{+\prime})$ $M4$-excitation cross sections for the lowest-energy states of maximum spin in p-shell nuclei. The fragmentation of the $M4$-transition strength into a large number of excited states is one of the principal sources of the widely discussed suppression effect, i.e., the noncorrespondence of the experimental values of the transition strengths with their estimates from simplified model approximations. The inclusion of the spread of the transition strength together with the evaluation of the single-particle density $\langle j_f \| j_3(qr)[Y_3 \times \sigma]_4 \| j_i \rangle$ on the basis of realistic nucleon wave functions in a well of finite depth apparently solves the problem of suppression of $M4$ excitations. The possibility of a quantitative interpretation of the distribution of $M4$-transition strengths as the result of the interaction of the nucleon degrees of freedom of the nucleus is evidence in favor of the need to make a detailed study of the role of the interaction of nucleon configurations in the formation of the structure and properties of the cross sections of different multipole order. Therefore, the study of $M4$ excitations decisively confirms the enormous possibilities offered by the multiparticle shell model for describing the properties of excited nuclear states. On the other hand, the comparison of the results of the theoretical calculation of the spectroscopic amplitudes of $M4$ excitations with the experimental values of these quantities reveals the limits of the traditional shell-model description. It becomes obvious that the set of values of the isoscalar and isovector MJ_{max}-transition amplitudes cannot be adequately reproduced using a model in which the wave functions are calculated with a set of phenomenological parameters from nuclear physics at low energies and momentum transfers. The amount of information contained in the experimental values of the spectroscopic amplitudes of the MJ_{max} transitions of a group of nuclei is large enough that the inverse problem can be proposed: the extraction of the configuration structure of the wave functions of excited states from the spectroscopic amplitudes and the determination of the parameters of the interaction responsible for formation of the excitation function.

[1)]We use the definition of the reduced matrix element

$$\langle j_1 m_1 | \hat{O}_{JM} | j_2 m_2 \rangle = \frac{\langle j_2 m_2 JM | j_1 m_1 \rangle}{\sqrt{2j_1+1}} \langle j_1 \| \hat{O}_J \| j_2 \rangle.$$

[1] R. A. Lindgren and F. Petrovich, in *Spin Excitations in Nuclei*, edited by F. Petrovich *et al.* (Plenum Press, New York, 1984), p. 323.
[2] T. W. Donnelly, J. D. Walecka, I. Sick *et al.*, Phys. Rev. Lett. **21**, 1196 (1968).
[3] T. de Forest and J. D. Walecka, Adv. Phys. **15**, 57 (1966).
[4] T. W. Donnelly and J. D. Walecka, Ann. Rev. Nucl. Sci. **25**, 325 (1975).
[5] I. S. Towner, Phys. Rep. **155**, 263 (1987).
[6] T. W. Donnelly, Phys. Rev. C **1**, 833 (1970).
[7] F. Petrovich, R. H. Howell *et al.*, Nucl. Phys. **A383**, 355 (1982).
[8] F. Petrovich, J. A. Carr, and H. McManus, Ann. Rev. Nucl. Part. Sci. **36**, 29 (1986).
[9] W. Bertozzi, Nucl. Phys. **A374**, 109c (1982).
[10] B. L. Clausen, R. A. Lindgren *et al.*, Phys. Rev. Lett. **65**, 547 (1990).
[11] S. Yen, R. Sobie *et al.*, Phys. Rev. C **27**, 1939 (1983).
[12] B. D. Anderson, J. D. Watson *et al.*, Phys. Lett. **123B**, 383 (1983).
[13] B. D. Anderson, A. Fasely *et al.*, in *Spin Excitations in Nuclei*, edited by F. Petrovich *et al.* (Plenum Press, New York, 1984), p. 391.
[14] R. A. Lindgren, W. J. Gerace *et al.*, Phys. Rev. Lett. **42**, 1524 (1979).
[15] R. A. Lindgren, C. F. Williamson, and S. Kovalski, Phys. Rev. Lett. **40**, 504 (1978).
[16] R. A. Lindgren, F. Petrovich *et al.*, Phys. Rev. C **14**, 1789 (1976).
[17] R. A. Lindgren, M. A. Plum *et al.*, Phys. Rev. Lett. **47**, 1266 (1981).
[18] R. A. Lindgren, J. B. Flanz *et al.*, Phys. Rev. Lett. **46**, 706 (1981).
[19] M. Rho, in *Spin Excitations in Nuclei*, edited by F. Petrovich *et al.* (Plenum Press, New York, 1984), pp. 111, 249.
[20] R. A. Lindgren, M. Leuschner *et al.*, Can. J. Phys. **65**, 666 (1987).
[21] A. M. Lallena, J. S. Dehesa, and S. Krewald, Phys. Rev. C **34**, 332 (1986).
[22] D. J. Millener and D. Kurath, Nucl. Phys. **A255**, 315 (1975); D. J. Millener, private communication.
[23] M. A. Plum, R. A. Lindgren *et al.*, Phys. Rev. C **40**, 1861 (1989).
[24] F. Petrovich and W. G. Love, Nucl. Phys. **A354**, 499c (1981).
[25] D. B. Holtcamp, S. J. Seestrom-Morris *et al.*, Phys. Rev. C **31**, 957 (1985).
[26] S. J. Seestrom-Morris, D. B. Holtcamp *et al.*, in *Spin Excitations in Nuclei*, edited by F. Petrovich *et al.* (Plenum Press, New York, 1984), p. 291.
[27] W. C. Love, M. A. Franey, and F. Petrovich, *ibid.*, p. 205.
[28] D. B. Holtcamp, S. J. Seestrom-Morris *et al.*, Phys. Rev. Lett. **45**, 420 (1980).
[29] I. Sick, E. B. Hughes *et al.*, Phys. Rev. Lett. **23**, 1117 (1969).
[30] C. Hyde, W. Bertozzi *et al.*, Bull. Am. Phys. Soc. **26**, 27 (1981).
[31] R. S. Henderson, B. M. Spicer *et al.*, Aust. J. Phys. **32**, 411 (1979).
[32] J. A. Carr, F. Petrovich *et al.*, Phys. Rev. C **27**, 1636 (1983).
[33] W. B. Cottingame, K. G. Boyer *et al.*, Phys. Rev. C **36**, 230 (1987).
[34] R. S. Hicks, J. B. Flanz *et al.*, Phys. Rev. C **30**, 1 (1984).
[35] R. S. Hicks, R. A. Lindgren *et al.*, Phys. Rev. C **34**, 1161 (1986).
[36] M. A. Plum, R. A. Lindgren *et al.*, Phys. Lett. **137B**, 15 (1984).
[37] J. C. Bergstrom, R. Neuhausen, and G. Lahm, Phys. Rev. C **29**, 1168 (1984).
[38] S. J. Seestrom-Morris, D. Denhard, and C. L. Morris, Phys. Rev. C **31**, 923 (1985).
[39] D. S. Koltun, in *Advances in Nuclear Science*, edited by A. Baranger and E. Vogt (New York, 1969), Vol. B, p. 71.
[40] B. S. Ishkhanov, I. M. Kapitonov *et al.*, Fiz. Elem. Chastits At. Yadra **12**, 905 (1981) [Sov. J. Part. Nucl. **12**, 362 (1981)].
[41] N. G. Goncharova, H. R. Kissener, and R. A. Éramzhyan, Fiz. Elem. Chastits At. Yadra **16**, 773 (1985) [Sov. J. Part. Nucl. **16**, 337 (1985)].
[42] H. R. Kissener, I. Rotter, and N. G. Goncharova, Fortschr. Phys. **35**, 277 (1987).
[43] H. U. Jager, H. R. Kissener, and R. A. Eramzhyan, Nucl. Phys. **A171**, 16 (1971).
[44] W. D. Teeters and D. Kurath, Nucl. Phys. **A275**, 61 (1977); **A283**, 1 (1977).
[45] H. R. Kissener, Dissertation, Dresden (1981).
[46] N. G. Goncharova and N. P. Yudin, Phys. Lett. **29B**, 272 (1969).
[47] S. Cohen and D. Kurath, Nucl. Phys. **73**, 1 (1965).
[48] S. Cohen and D. Kurath, Nucl. Phys. **A101**, 1 (1967).
[49] G. van der Steenhoven, H. P. Blok *et al.*, Nucl. Phys. **A480**, 547 (1988).
[50] N. G. Goncharova, B. S. Ishkhanov, and V. I. Mokeev, Yad. Fiz. **35**, 43 (1982) [Sov. J. Nucl. Phys. **35**, 26 (1982)].
[51] A. N. Gol'tsov and N. G. Goncharova, Yad. Fiz. **38**, 1410 (1983) [Sov. J. Nucl. Phys. **38**, 857 (1983)].
[52] N. G. Goncharova and G. S. Sagiyan, Vestn. Mosk. Univ. Ser. Fiz. **13**, 121 (1972) [in Russian].
[53] N. Goncharova, Czech J. Phys. B **32**, 225 (1982).
[54] N. G. Goncharova, A. N. Golzov, and H. R. Kissener, Nucl. Phys. **A462**, 367 (1987).
[55] A. N. Golzov, N. G. Goncharova, and H. R. Kissener, Nucl. Phys. **A462**, 378 (1987).
[56] N. G. Goncharova, V. J. Spevak, and H. R. Kissener, Nucl. Phys. **A516**, 15 (1990).
[57] N. G. Goncharova, H. R. Kissener, and R. A. Eramzhyan, Izv. Akad. Nauk SSSR, Ser. Fiz. **50**, 996 (1985) [Bull. Acad. Sci. USSR, Phys. Ser.].
[58] N. G. Goncharova, Yad. Fiz. **51**, 1281 (1990) [Sov. J. Nucl. Phys. **51**, 814 (1990)].
[59] É. R. Arakelyan and N. G. Goncharova, Yad. Fiz. **54**, 920 (1991) [Sov. J. Nucl. Phys. **54**, 557 (1991)].
[60] V. Gillet and N. Vinh-Mau, Nucl. Phys. **54**, 321 (1964).
[61] R. S. Allas, S. S. Hanna *et al.*, Nucl. Phys. **58**, 122 (1964).
[62] É. R. Arakelyan and N. G. Goncharova, in *Abstracts from the Forty-Second Meeting on Nuclear Spectroscopy* [in Russian], Alma-Ata, 1992.
[63] H. Bagheai, R. A. Lindgren *et al.*, IUCF Newsletters, April, 1990, p. 10.
[64] B. Zeideman, D. F. Geesaman *et al.*, Phys. Rev. C **38**, 2251 (1988).
[65] F. Ajzenberg-Selove, Nucl. Phys. **A490**, 1 (1988).
[66] C. L. Morris, J. Piffaretti, and H. A. Thiessen, Phys. Lett. **86B**, 31 (1979).
[67] B. L. Clausen, R. J. Peterson, and R. A. Lindgren, Phys. Rev. C **38**, 589 (1988).
[68] A. N. Gol'tsov and N. G. Goncharova, Izv. Akad. Nauk SSSR, Ser. Fiz. **50**, 996 (1986) [Bull. Acad. Sci. USSR, Phys. Ser.].
[69] U. Kneissl, K. Leister *et al.*, Nucl. Phys. **A264**, 30 (1976).
[70] N. G. Goncharova and V. Ya. Spevak, Izv. Akad. Nauk SSSR, Ser. Fiz. **53**, 917 (1989) [Bull. Acad. Sci. USSR, Phys. Ser.].
[71] B. H. Patrick *et al.*, J. Phys. G **2**, 751 (1976).
[72] T.-S. H. Lee and D. Kurath, Phys. Rev. C **21**, 293 (1980); **22**, 1670 (1980).

Translated by Patricia A. Millard